using analysis of variance with Bonferroni/Dunn protected least significant difference ($p < 0.01$).

Analysis of Cell Death Pathway

To determine the pathways involved in apoptosis in the SV as a results of CDDP toxicity, immunohistochemistry for cleaved caspase-3, -8, -9 or cytochrome c was performed in CDDP-treated or control specimens obtained on day 3. Rabbit polyclonal antibodies against cleaved caspase-3 (1:50; Cell Signaling Technology, Beverly, Mass., USA), cleaved caspase-9 (1:100; Cell Signaling Technology), cytochrome c (1:500; Santa Cruz Biotechnology, Santa Cruz, Calif., USA), mouse monoclonal antibody against cleaved caspase-8 (1:50; Cell Signaling Technology) and goat polyclonal antibody against AIF (1:100, Santa Cruz Biotechnology) were used as the primary antibodies. Alexa-Fluor 594-conjugated goat antirabbit or antimouse IgG (1:200; Molecular Probes) or Alexa-Fluor 594-conjugated donkey antigoat IgG (1:200; Molecular Probes) was used as the secondary antibody. Counterstaining with DAPI was performed to demonstrate nuclear morphology. Expression of these molecules and their cellular location in apoptotic marginal cells was compared with that in normal marginal cells using a Nikon ECLIPSE E600 fluorescence microscope.

Generation of Reactive Radical Species

To examine the involvement of reactive oxygen species in CDDP-induced degeneration of the SV, the expression of NT and HNE was evaluated using immunohistochemistry. Rabbit anti-NT polyclonal antibody (1:100; Upstate Biotechnology, Lake Placid, N.Y., USA) or mouse anti-HNE monoclonal antibody (1:8; Oxis Research, Portland, Oreg., USA) was used as the primary antibody. Specimens were incubated overnight at 4 °C with the appropriate primary antibody then washed with PBS three times and incubated for 1 h at room temperature with the secondary antibody. Rhodamine-conjugated donkey antirabbit IgG (1:500; Chemicon, Temecula, Calif., USA) or Alexa-Fluor 594-conjugated goat antimouse IgG (1:200; Molecular Probes) was used as the secondary antibody. Generation of NO was indirectly evaluated using analysis of iNOS activity. To determine NOS activity in the SV, immunohistochemistry for iNOS was employed. Rabbit anti-iNOS polyclonal antibody (1:20; BD Biosciences, San Jose, Calif., USA) was used as the primary antibody. Alexa-Fluor 594-conjugated goat antirabbit IgG (1:200; Molecular Probes) was used as the secondary antibody.

Results

Estimation of Stria Degeneration

HE staining revealed degenerative changes in the SV following CDDP treatment. On day 3 after treatment, edematous swelling was observed in the SV (fig. 1b), while atrophic changes were found on days 7 and 14 (fig. 1c, d). Control specimens obtained on day 3 or day 14 showed normal morphology (fig. 1a). The thickness of the SV on days 7 and 14 was much reduced compared with that of controls and quantitative analysis of the SV area supported this morphological observation. A significant decrease in the area of the SV was observed on days 7 and 14 (fig. 1m). In age-matched controls, no degenerative changes in the SV were observed. TUNEL staining demonstrated a rapid induction of apoptotic cell death in the SV after CDDP application (fig. 1e–h). Age-matched controls exhibited no TUNEL-positive cells in the SV. In specimens obtained on day 3, numerous TUNEL-positive cells were found in the SV (fig. 1f), with the majority located in the layer of marginal cells. TUNEL-positive cells were also observed in the SV on days 7 and 14, although they were limited in numbers. No TUNEL-positive cells were observed in control specimens. Quantitative analysis of TUNEL-positive cells in the SV clarified the time course of induction of apoptosis following CDDP treatment (fig. 1n). Merged DAPI fluorescence and bright-field images demonstrated a decrease in cell numbers in the cochlear lateral wall including the SV (fig. 1i–l). Quantitative assessment of cell numbers in the SV revealed a significant decrease in cell numbers between day 3 and day 7 (fig. 1o), corresponding to the induction of TUNEL-positive cells on day 3.

Analysis of Cell Death Pathways

Expression of apoptosis-related molecules in apoptotic marginal cells on day 3 was compared with that in healthy marginal cells in age-matched controls. Marginal cells affected by CDDP exhibited expression of cleaved caspase-3 (fig. 2b), while none was observed in marginal cells in controls (fig. 2a). In specimens obtained on day 3 after CDDP administration, a majority of marginal cells were positive for cleaved caspase-3. In contrast, there was no expression of cleaved caspase-8 in either control or CDDP-treated specimens (fig. 2c, d). Expression of cleaved caspase-9 was found in about 50% of marginal cells (fig. 2f), while normal marginal cells exhibited no expression (fig. 2e). No expression of AIF was found in either control or CDDP-treated specimens (fig. 2g, h). On the other hand, immunohistochemistry for cytochrome c indicated release of cytochrome c from the mitochondria into the cytoplasm in affected marginal cells. Marginal cells in controls exhibited expression of cytochrome c, which was extruded from the nuclear space, in the cytoplasm (fig. 3a–c). In contrast, marginal cells damaged by CDDP exhibited a weak and diffuse distribution of cytochrome c in the cytoplasm including the nuclear spaces (fig. 3d–f).

Generation of Reactive Radical Species

Immunohistochemistry for HNE demonstrated the occurrence of lipid peroxidation in the SV and spiral ligament (SL) after CDDP treatment (fig. 4a–d). In controls,

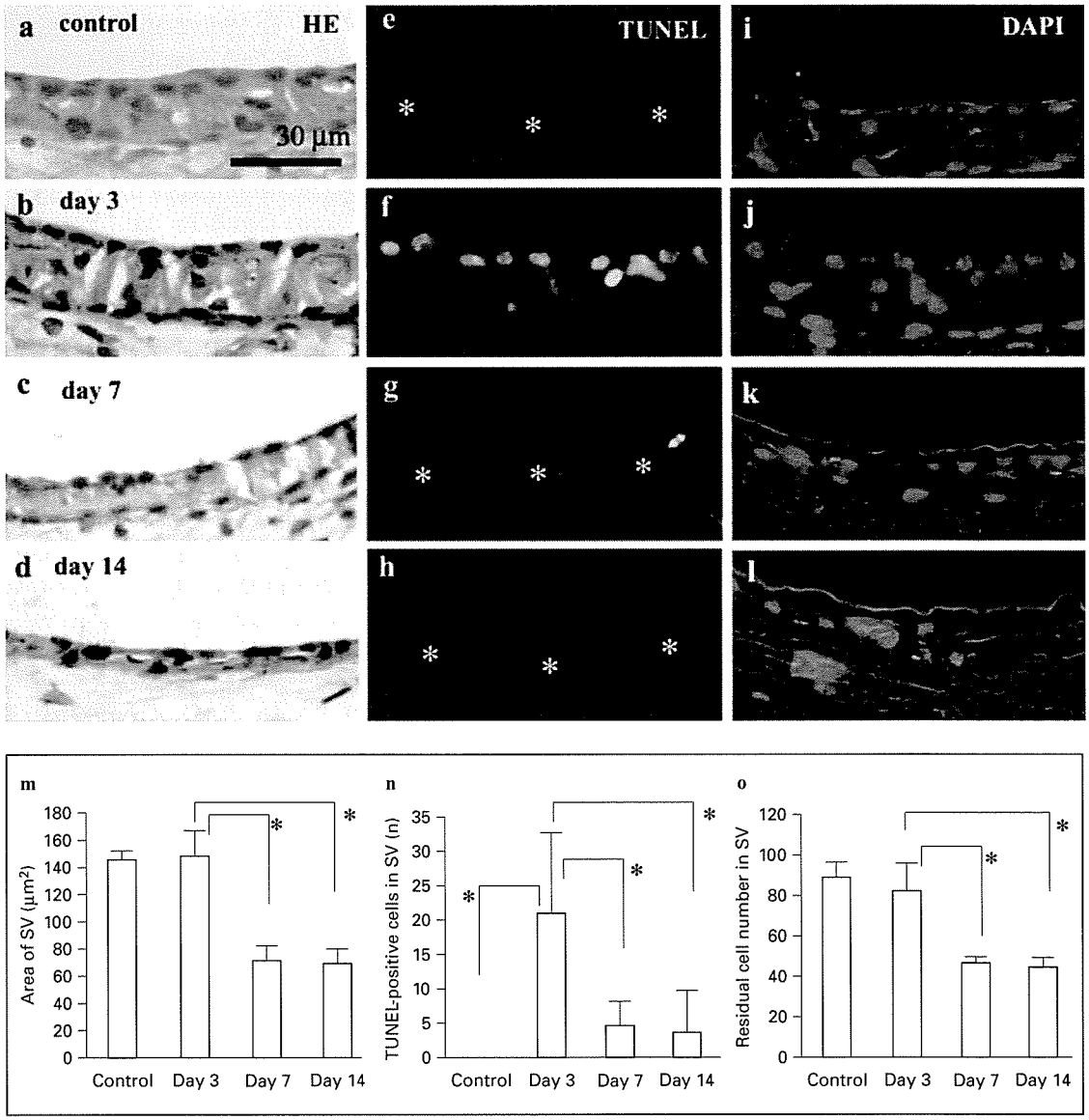

Fig. 1. Degeneration of the SV of the second turn of cochleae following CDDP treatment. HE staining (**a–d**) showing edematous swelling of the SV on day 3 (**b**) and progressive atrophy on days 7 (**c**) and 14 (**d**). TUNEL staining (green; **e–h**) showing predominant induction of apoptotic cell death in the SV on day 3 (**f**). Asterisks indicate the location of the SV. Combined images of DAPI fluorescence (blue) and bright fields (**i–l**) showing an apparent decrease in cell numbers in the SV on days 7 (**k**) and 14 (**l**). Bar represents 30 µm. Quantitative assessment of areas of the SV of the second turn of cochleae demonstrates a significant decrease in areas on day 7 and 14 (**m**). **n** Mean numbers of TUNEL-positive cells in the SV. Predominant induction of TUNEL labeling is observed on day 3. Residual cell numbers in the SV significantly decrease on days 7 and 14 (**o**). Bars represent standard deviations. Statistical significance is determined by ANOVA with Bonferroni/Dunn test for significance (* $p < 0.0083$).

no positive staining for HNE was found in the SV or the SL (fig. 4a). In specimens obtained on day 3, the SV and SL both exhibited strong expression of HNE on their cytoplasmic membrane (fig. 4b), with no differences in immunoreactivity between the SV and SL. In contrast, the SV exhibited weak expression of HNE on days 7 and 14, although strong expression of HNE remained in the SL (fig. 4c, d).

Immunohistochemistry for NT verified the occurrence of protein peroxidation by peroxynitrite in the SV and SL

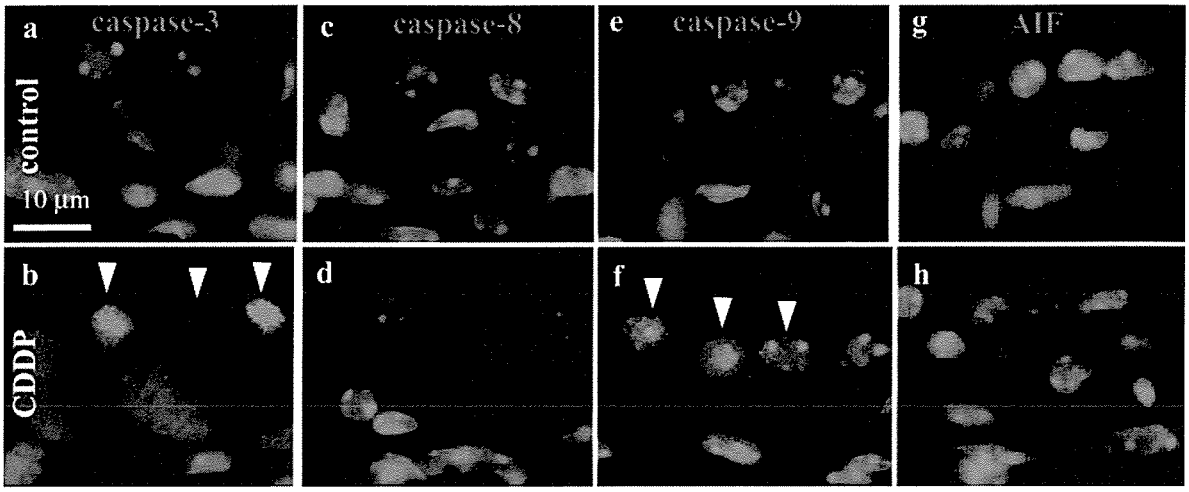

Fig. 2. Immunohistochemistry for apoptosis-related proteins in the SV of control specimens obtained on day 3 and of CDDP-treated specimens also obtained on day 3. In control specimens, no expression of cleaved caspase-3, -8, -9 or AIF is found in the SV (**a**, **c**, **e**, **g**). Damaged marginal cells express cleaved caspase-3 (arrowheads; **b**) and caspase-9 (arrowheads; **f**), but not cleaved caspase-8 (**d**) or AIF (**h**). Blue indicates counterstaining with DAPI. Bar represents 10 μm.

(fig. 4e–h). In controls, faint or no expression of NT was observed in the SV (fig. 4e). In contrast, CDDP-treated specimens exhibited striking expression of NT in the SV on days 3 and 7 (fig. 4f, g). Specimens on day 14 exhibited weak expression of NT in the SV (fig. 4h). The SL exhibited expression of NT in all CDDP-treated specimens.

In controls, there was no expression of iNOS in the SV and SL (fig. 4i). However, strong expression of iNOS was identified in the SV on day 3 (fig. 4j). In specimens obtained on day 7, expression of iNOS in the SV was moderate (fig. 4k). On day 14, only faint expression of iNOS was observed in the SV (fig. 4l). The SL of CDDP-treated animals exhibited weak expression of iNOS.

Discussion

Cell Death Model for the SV

In the present study, local application of CDDP into the inner ear of mice caused degeneration of the SV. The method for local application of ototoxic agents into the mouse inner ear has been reported [18]. A single injection of CDDP into the semicircular canal induces degeneration of cochlear hair cells [19] and spiral ganglions [20]. Degeneration of spiral ganglions has been found from the basal to apical portion of cochleae. These findings suggest that CDDP administrated from the semicircular canal reaches to the apical portion of cochleae.

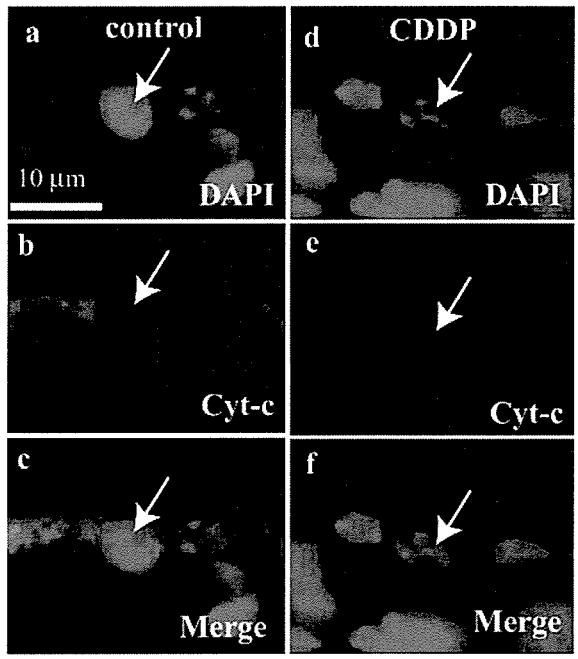

Fig. 3. Immunohistochemistry for cytochrome c (Cyt-c) of the SV of control specimens obtained on day 3 (**a–c**) and CDDP-treated specimen also obtained on day 3 (**d–f**). **a**, **d** Nuclear staining with DAPI. **b**, **e** Immunohistochemistry for Cyt-c. **c**, **f** Merged images. The distribution of Cyt-c in marginal cells of the control is clearly extruded from nuclear spaces (**a–c**, arrows), while that of the CDDP-treated specimen is diffuse throughout their nuclear spaces (**d–f**, arrows). Bar represents 10 μm.

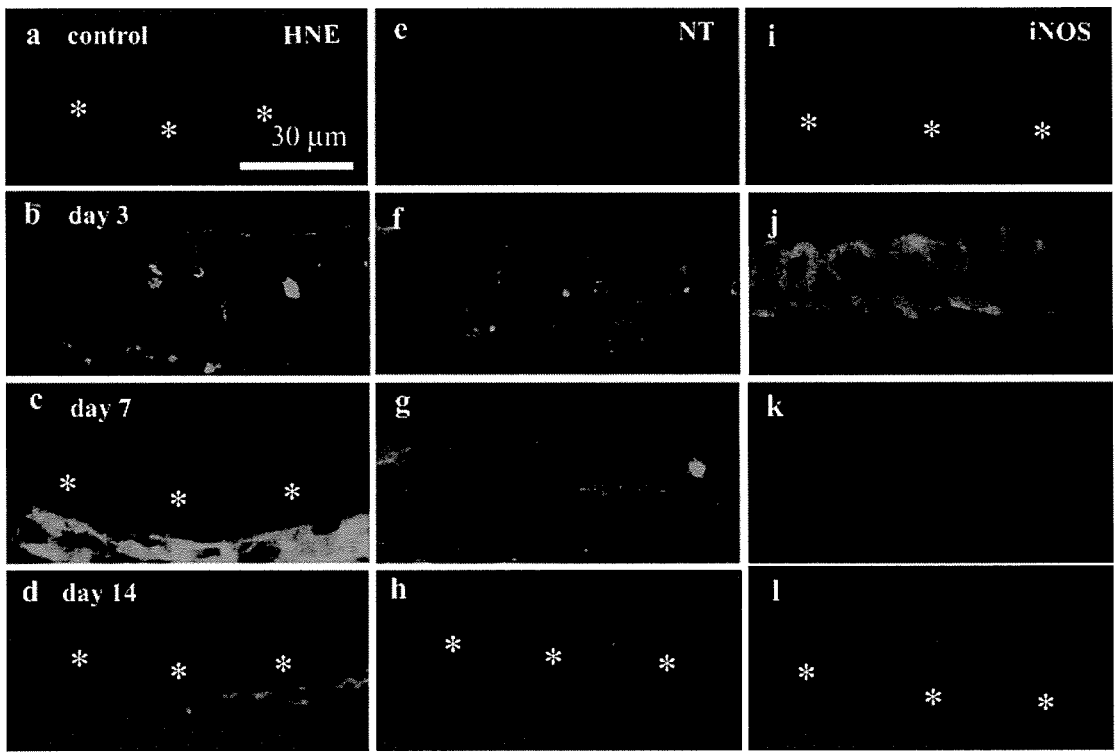

Fig. 4. Expression of HNE, NT and iNOS in the SV of the second turn of cochleae following CDDP treatment. Immunostaining for HNE (**a–d**) showing expression of HNE in the SV and SL following CDDP treatment (**b–d**). Strong expression in the SV on day 3 is noted (**b**). Immunostaining for NT (**e–h**) showing intense staining in the SV on days 3 (**f**) and 7 (**g**). Immunostaining for iNOS (**i–l**) showing expression of iNOS in the SV on days 3 (**j**) and 7 (**k**). Asterisks indicate the location of the SV. Bar represents 30 μm.

Morphologically, edema formation in the SV appeared during the early phase of degeneration after CDDP treatment, followed by severe atrophy during the late phase. The time course of morphological changes of the SV observed in this study was similar to that observed in previous studies using systemic CDDP application [3–5]. TUNEL assays revealed induction of apoptotic cell death in the SV after CDDP treatment. Most TUNEL-positive cells were located in the marginal cell layer of the SV, in agreement with previous findings using systemic administration of CDDP [9, 21]. The present findings demonstrate that apoptotic cells in the SV appeared predominantly on day 3 following CDDP treatment. The predictability of the induction of apoptotic cell death in the SV makes this an ideal system in which to study cell death mechanisms. In addition, there was a significant reduction in the area of the SV following induction of apoptotic cell death. Since marginal cells constitute a major part of the SV [5], their loss leads to a large reduction in the area of the SV.

Cell Death Pathways in Marginal Cells

Expression of proteins associated with apoptosis was examined using specimens obtained on day 3 after CDDP or control treatment. Day 3 was chosen as this was the day on which induction of apoptosis in marginal cells was most likely to be observed. Apoptosis is caused by a complicated cascade of pathways (fig. 5). The majority of marginal cells affected by CDDP exhibited expression of cleaved caspase-3, similar to the previous findings [22]. This indicates that caspases are involved in the process of apoptotic cell death in marginal cells following CDDP treatment. Activation of caspase-3 leads to activation of a series of caspases [23]. On the other hand, expression of AIF was not found in damaged marginal cells, which supports the hypothesis that the caspase family plays a central role in the degradation of marginal cells affected by CDDP. Apoptotic signaling is initiated by activation of the death receptor mediated by damage to the mitochondrial membrane or stress to the endoplasmic reticulum (fig. 5). In this study, damaged marginal cells exhibited no

expression of cleaved caspase-8, indicating that the death receptor-mediated pathway is not a major pathway of apoptotic cell death in these cells after treatment with CDDP. However, expression of cleaved caspase-9 was observed in damaged marginal cells. In addition, immunohistochemistry for cytochrome c showed that there was release of cytochrome c from the mitochondria to the cytoplasm in damaged marginal cells. These findings indicate that the majority of damaged marginal cells die via apoptosis initiated by permeabilization of mitochondrial membranes. However, expression of activated caspase-9 was not observed in all of the affected marginal cells. Therefore, there is a possibility that other apoptotic pathways activate caspase-3 in damaged marginal cells. Recent studies have indicated that the mode of action of CDDP involves endoplasmic reticulum stress [24]. It is believed that endoplasmic reticulum stress results in release of calpain which in turn activates caspase-12 leading to activation of caspase-3 (fig. 5) [11]. In addition, carboplatin, a second-generation cisplatin analogue, reportedly causes activation of calpain in nerve fibers in the inner ear [25]. Overall, further studies are required in order to define the signaling pathways involved in CDDP-induced apoptosis of marginal cells.

Reactive Radical Species in Damage of Marginal Cells

Immunohistochemical analysis demonstrates that CDDP induced production of NT and HNE in the SV, indicating the occurrence of protein peroxidation by peroxynitrite and lipid peroxidation by hydroxy radicals in the SV. Notably, strong expression of these two molecules in the SV was observed on day 3 when apoptosis of marginal cells was most likely to be induced. In addition, expression of both molecules in the SV became weaker when the numbers of apoptotic cells in the SV decreased. These findings suggest that peroxynitrite and hydroxy radicals are involved in the induction of apoptotic cell death in the SV. Moreover, both peroxynitrite and HNE have been shown to induce mitochondrial membrane permeabilization [26]. Immunohistochemical analysis for caspases and apoptosis-related proteins indicated that damage to mitochondria might play a key role in the induction of apoptotic death of marginal cells. Therefore, both peroxynitrite and hydroxy radicals may be mediators for induction of apoptosis by CDDP in marginal cells. Peroxynitrite is formed by the reaction of NO with superoxide (fig. 6) [15]. NO is produced by a group of enzymes called NOS. Mammalian systems contain three well-characterized isoforms of NOS. Amongst the three isoforms of NOS, iNOS shows the highest activity. In fact,

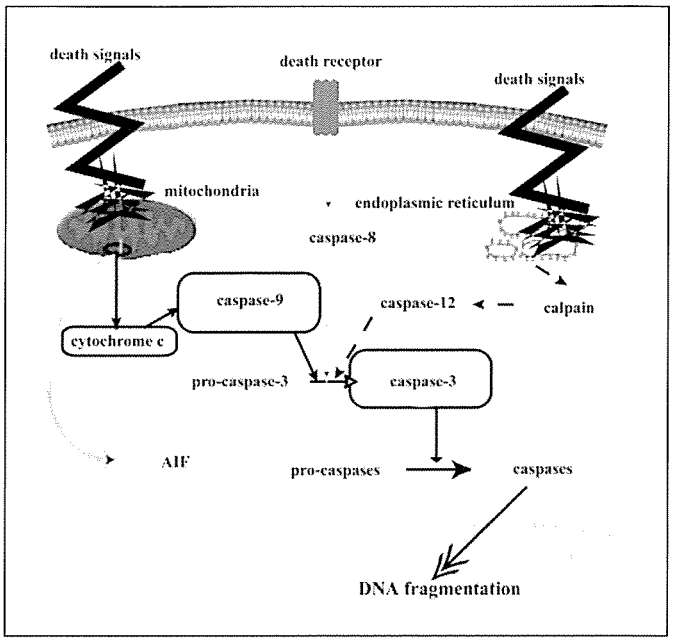

5

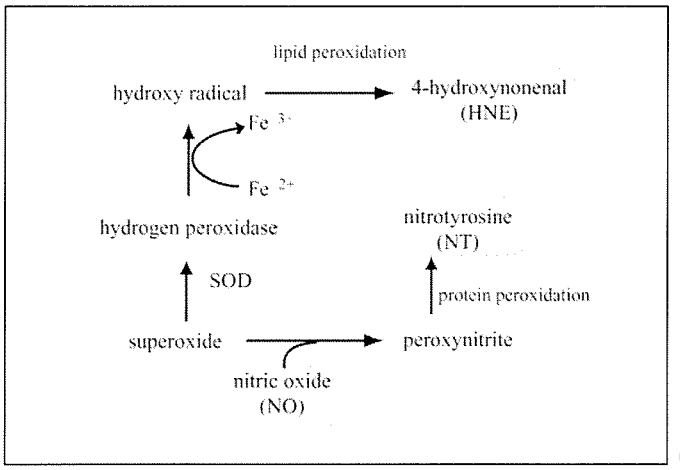

6

Fig. 5. Schematic diagram showing the pathways of apoptosis.
Fig. 6. Generation of reactive radical species and their products. SOD = Superoxide dismutase.

overproduction of NO by iNOS is implicated in a number of pathogenic conditions [27] including CDDP-induced degeneration of the SV [28]. Thus, we have examined expression of iNOS in the SV following CDDP treatment. The pattern of expression of iNOS in the SV appears to follow the same time course as that of NT in this study. In fact, overproduction of NO by iNOS may be linked with generation of peroxynitrite in the SV. We suggest that inhibition of iNOS activity may therefore be a cue for protection of the SV from CDDP toxicity.

The present findings have shown that there is generation of HNE in the SV following CDDP treatment, indicating generation of hydroxy radicals. It has been shown that hydroxy radical peroxidation of polyunsaturated fatty acids in cellular membranes results in the production of HNE (fig. 6), which causes further lipid peroxidation and acts as a pro-apoptotic mediator [26]. Therefore, inhibition of hydroxy radical generation is crucial for stopping this chain reaction. Superoxide is metabolized to hydroxy radicals in the presence of iron ions [17]. In addition, superoxide can form peroxynitrite by reaction with NO (fig. 6). Therefore, inhibition of the production of hydroxy radicals from superoxide may result in an increase in peroxynitrite. Reduction of both hydroxy radicals and peroxynitrite by, for example, treatment with an iNOS inhibitor and a hydroxy radical scavenger may be effective for the protection of the SV from CDDP toxicity.

The present findings suggest that CDDP toxicity causes apoptosis initiated by mitochondrial damage in the SV. Apoptosis occurs mainly in marginal cells and is mediated by the formation of peroxynitrite and hydroxy radicals. We suggest that reduction of these reactive radical species may lead to stabilization of mitochondrial membrane permeability, leading to protection of the SV from CDDP toxicity.

Acknowledgements

We are grateful to J. Schacht for helpful suggestions and to Z. Taniguchi, K. Yuki, S. Tamura, A. Toyota, T. Tsukamoto and K. Fujita for technical assistance. This study was supported by a grant-in-aid for scientific research, a grant-in-aid for exploratory research and a grant-in-aid for regenerative medicine realization project from the Ministry of Education, Science, Sports, Culture and Technology of Japan.

References

1 Hoeve LJ, Mertens zur Borg IR, Rodenburg M, Brocaar MP, Groen BG: Correlations between cis-platinum dosage and toxicity in a guinea pig model. Arch Otorhinolaryngol 1988;245:98–102.
2 Waters GS, Ahmad M, Katsarkas A, Stanimir G, McKay J: Ototoxicity due to cis-diamminedichloroplatinum in the treatment of ovarian cancer: Influence of dosage and schedule of administration. Ear Hear 1991;12:91–102.
3 Tange RA, Vuzevski VD: Changes in the stria vascularis of the guinea pig due to cis-platinum. Arch Otorhinolaryngol 1984;239:41–47.
4 Kohn S, Fradis M, Pratt H, Zidan J, Podoshin L, Robinson E, Nir I: Cisplatin ototoxicity in guinea pigs with special reference to toxic effects in the stria vascularis. Laryngoscope 1988;98:865–871.
5 Meech RP, Campbell KC, Hughes LP, Rybak LP: A semiquantitative analysis of the effects of cisplatin on the rat stria vascularis. Hear Res 1998;124:44–59.
6 Offner FF, Dallos P, Cheatham MA: Positive endocochlear potential; Mechanism of production by marginal cells of stria vascularis. Hear Res 1987;29:117–124.
7 Forge A: Outer hair cell loss and supporting cell expansion following chronic gentamicin treatment. Hear Res 1985;19:171–182.
8 Nakagawa T, Yamane H, Shibata S, Nakai Y: Gentamicin ototoxicity induced apoptosis of the vestibular hair cells of guinea pigs. Eur Arch Otorhinolaryngol 1997;254:9–14.
9 Alam SA, Ikeda K, Oshima T, Suzuki M, Kawase T, Kikuchi T, Takasaka T: Cisplatin-induced apoptotic cell death in Mongolian gerbil cochlea. Hear Res 2000;141:28–38.
10 Cohen GM: Caspases: The executioners of apoptosis. Biochem J 1997;326:1–16.
11 Li P, Nijhawan D, Budihardjo I, Srinivasula SM, Ahmad M, Alnemri ES, Wang X: Cytochrome c and dATP-dependent formation of Apaf-1/caspase-9 complex initiates an apoptotic protease cascade. Cell 1997;91:479–489.
12 Nakagawa T, Yuan J: Cross-talk between two cysteine protease families; Activation of caspase-12 by calpain in apoptosis. J Cell Biol 2000;150:887–894.
13 Susin SA, Lorenzo HK, Zamzami N, et al: Molecular characterization of mitochondrial apoptosis-inducing factor. Nature 1999;397:441–446.
14 Evans P, Halliwell B: Free radicals and hearing. Cause, consequence, and criteria. Ann NY Acad Sci 1999;884:19–40.
15 Groves JT: Peroxynitrite: Reactive, invasive and enigmatic. Curr Opin Chem Biol 1999;3:226–235.
16 Nakazawa H, Fukuyama N, Takizawa S, Tsuji C, Yoshitake M, Ishida H: Nitrotyrosine formation and its role in various pathological conditions. Free Radic Res 2000;33:771–784.
17 Esterbauer H, Schaur RJ, Zollner H: Chemistry and biochemistry of 4-hydroxynonenal, malonaldehyde and related aldehydes. Free Radic Biol Med 1991;11:81–128.
18 Nakagawa T, Kim TS, Murai N, et al: A novel technique for inducing local inner ear damage. Hear Res 2003;176:122–127.
19 Lee JE, Nakagawa T, Kim TS, Endo T, Shiga A, Iguchi F, Lee SH, Ito J: Role of reactive radicals in degeneration of the auditory system of mice following cisplatin treatment. Acta Otolaryngol, in press.
20 Lee JE, Nakagawa T, Kim TS, Iguchi F, Endo T, Dong Y, Yuki K, Naito Y, Lee SH, Ito J: A novel model for rapid induction of apoptosis in spiral ganglions of mice. Laryngoscope 2003;113:949–999.
21 Teranishi M, Nakashima T, Wakabayashi T: Effects of alpha-tocopherol on cisplatin-induced ototoxicity in guinea pigs. Hear Res 2001;151:61–70.
22 Watanabe K, Inai S, Jinnouchi K, Baba S, Yagi T: Expression of caspase-activated deoxyribonuclease (CAD) and caspase 3 (CPP32) in the cochlea of cisplatin (CDDP)-treated guinea pigs. Auris Nasus Larynx 2003;30:219–225.
23 Kumar S: The apoptotic cysteine protease CPP32. Int J Biochem Cell Biol 1997;29:393–396.
24 Mandic A, Hansson J, Linder S, Shoshan MC: Cisplatin induces endoplasmic reticulum stress and nucleus-independent apoptotic signaling. J Biol Chem 2003;278:9100–9106.
25 Ding L, McFadden SL, Salvi RJ: Calpain immunoreactivity and morphological damage in chinchilla inner ears after carboplatin. J Assoc Res Otolaryngol 2002;3:68–79.
26 Vieira HL, Belzacq AS, Haouzi D, et al: The adenine nucleotide translocator: A target of nitric oxide, peroxynitrite, and 4-hydroxynonenal. Oncogene 2001;20:4305–4316.
27 Boje KM, Jaworowicz D Jr, Raybon JJ: Neuroinflammatory role of prostaglandins during experimental meningitis: Evidence suggestive of an in vivo relationship between nitric oxide and prostaglandins. J Pharmacol Exp Ther 2003;304:319–325.
28 Watanabe K, Inai S, Jinnouchi K, Bada S, Hess A, Michel O, Yagi T: Nuclear-factor kappa B (NF-kappa B)-inducible nitric oxide synthase (iNOS/NOS II) pathway damages the stria vascularis in cisplatin-treated mice. Anticancer Res 2002;22:4081–4085.

Article

Radixin deficiency causes deafness associated with progressive degeneration of cochlear stereocilia

Shin-ichiro Kitajiri,[1,2,3] Kanehisa Fukumoto,[1,4] Masaki Hata,[5] Hiroyuki Sasaki,[5,6] Tatsuya Katsuno,[1,7] Takayuki Nakagawa,[3] Juichi Ito,[3] Shoichiro Tsukita,[1,2] and Sachiko Tsukita[1,2,8]

[1]Department of Cell Biology, Faculty of Medicine, Kyoto University, Sakyo-ku, Kyoto 606-8501, Japan
[2]Solution Oriented Research for Science and Technology, Japan Science and Technology Corporation, Sakyo-ku, Kyoto 606-8501, Japan
[3]Department of Otolaryngology Head and Neck Surgery, Faculty of Medicine, Kyoto University, Sakyo-ku, Kyoto 606-8507, Japan
[4]Department of Surgery, Kyoto Prefectural University of Medicine, Kamigyo-ku, Kyoto 602-8566, Japan
[5]KAN Research Institute, Kyoto Research Park, Shimogyo-ku, Kyoto 606-8317, Japan
[6]Department of Molecular Cell Biology, Institute of DNA Medicine, The Jikei University School of Medicine, Nishi-Shinbashi, Minato-ku, Tokyo 105-8461, Japan
[7]Department of Biological Sciences and Institute for Advanced Research, Nagoya University, Nagoya 464-8602, Japan
[8]School of Health Sciences, Faculty of Medicine, Kyoto University, Sakyo-ku, Kyoto 606-8507, Japan

Ezrin/radixin/moesin (ERM) proteins cross-link actin filaments to plasma membranes to integrate the function of cortical layers, especially microvilli. We found that in cochlear and vestibular sensory hair cells of adult wild-type mice, radixin was specifically enriched in stereocilia, specially developed giant microvilli, and that radixin-deficient ($Rdx^{-/-}$) adult mice exhibited deafness but no obvious vestibular dysfunction. Before the age of hearing onset (~2 wk), in the cochlea and vestibule of $Rdx^{-/-}$ mice, stereocilia developed normally in which ezrin was concentrated. As these $Rdx^{-/-}$ mice grew, ezrin-based cochlear stereocilia progressively degenerated, causing deafness, whereas ezrin-based vestibular stereocilia were maintained normally in adult $Rdx^{-/-}$ mice. Thus, we concluded that radixin is indispensable for the hearing ability in mice through the maintenance of cochlear stereocilia, once developed. In $Rdx^{-/-}$ mice, ezrin appeared to compensate for radixin deficiency in terms of the development of cochlear stereocilia and the development/maintenance of vestibular stereocilia. These findings indicated the existence of complicate functional redundancy in situ among ERM proteins.

Introduction

Deafness is one of the most prevalent forms of sensory impairment in humans, and it affects ~1 in 1,000 children (for reviews see Morton, 1991; Fortnum and Davis, 1997). Various gene mutations are known to cause hereditary hearing loss in humans (for reviews see Holme and Steel, 1999; Petit et al., 2001; Tekin et al., 2001; Zuo, 2002). Hearing is achieved through a number of steps: first, acoustic stimuli reaching the cochlea deflect the stereocilia on the apical surface of the inner and outer hair cells in the organ of Corti, which in turn opens the mechanotransduction channels located at the tips of stereocilia. Potassium then floods through these open channels, resulting in plasma membrane depolarization, and an electrical signal is transmitted to the central nervous system (for reviews see Roberts et al., 1988; Hudspeth, 1989; Pickles and Corey, 1992). Thus, the stereocilia of cochlear hair cells are key elements in the transduction of acoustic stimuli into electrical signals. Stereocilia also occur in the hair cells of the vestibule to detect acceleration (Eatock et al., 1998; Corey, 2003). Deaf mouse models have provided crucial clues for understanding the molecular and cellular biology of cochlear sensory hair cells, and several forms of hearing loss are now understood to be caused by mutations of the cytoskeletal proteins of cochlear stereocilia (Probst and Camper, 1999; Gillespie and Walker, 2001; Steel and Kros, 2001; Call and Morton, 2002; Zuo, 2002; Belyantseva et al., 2003). In these mice, vestibular stereocilia were also defective, concomitantly causing imbalance.

Address correspondence to Sachiko Tsukita, Dept. of Cell Biology, Kyoto University Faculty of Medicine, Yoshida-Konoe, Sakyo-ku, Kyoto 606-8501, Japan. Tel.: (81) 75-753-4373. Fax: (81) 75-753-4660. email: atsukita@mfour.med.kyoto-u.ac.jp

Key words: ERM; radixin; stereocilia; cochlea; deafness

Abbreviations used in this paper: ABR, auditory-evoked brainstem response; dB, decibel; ERM, ezrin/radixin/moesin; SPL, sound pressure level; VOR, vestibulo-ocular reflex.

The Journal of Cell Biology, Volume 166, Number 4, August 16, 2004 559–570
http://www.jcb.org/cgi/doi/10.1083/jcb.200402007

Stereocilia are specifically developed giant microvilli (finger-like projections of plasma membrane that are underlain by actin filaments). Microvilli show significant variations in morphology, diameter, and length depending on cell types; some are formed by densely packed rigid-looking actin filaments, whereas others are formed by loosely packed fragile-looking actin filaments (Furukawa and Fechheimer, 1997; Bartles, 2000; DeRosier and Tilney, 2000). Of these microvilli, the stereocilia of cochlear sensory hair cells are the most specialized with a characteristic morphology (DeRosier et al., 1980; Gillespie and Walker, 2001; Zuo, 2002). The stereocilia of vestibular sensory hair cells show a more fragile appearance (Sobin and Flock, 1983; Denman-Johnson and Forge, 1999). Besides the general microvilli cytoskeletal proteins such as actin, fimbrin, and myosin Ic, which were immunolocalized to stereocilia (Tilney et al., 1989; Drenckhahn et al., 1991; Skowron et al., 1998; Dumont et al., 2002), the positional cloning of deafness genes in humans and mice has enabled the identification of the novel cytoskeleton-associated constituents of stereocilia such as espin, harmonin, SANS, whirlin, unconventional myosins (VI/VIIa/XV), and cadherins (cadherin 23 and protocadherin 15); these proteins are most likely implicated during stereocilia formation and/or maintenance (Avraham et al., 1995; Gibson et al., 1995; Probst et al., 1998; Liang et al., 1999; Littlewood Evans and Müller, 2000; Zheng et al., 2000; Alagramam et al., 2001; Di Palma et al., 2001; Wada et al., 2001; Boeda et al., 2002; Karolyi et al., 2003; Mburu et al., 2003; Weil et al., 2003). Despite these advances, we are still far from having a comprehensive view of how the stereocilia of hair cells are built during development and maintained throughout life.

Ezrin/radixin/moesin (ERM) proteins are three closely related proteins in the band 4.1 superfamily that are thought to function as cross-linkers between plasma membranes and actin filaments, thus integrating the actin cortical layer, especially the microvilli (Sato et al., 1992; Berryman et al., 1993; Mangeat et al., 1999; Tsukita and Yonemura, 1999; Bretscher et al., 2002). The COOH-terminal domains of these ERM proteins bind to the actin filaments (Algrain et al., 1993; Turunen et al., 1994; Martin et al., 1995), and the NH_2-terminal halves, the FERM domains (band 4.1/ezrin/radixin/moesin homology domains; Algrain et al., 1993; Henry et al., 1995; Bretscheret al., 2002), associate directly with the cytoplasmic domains of several integral membrane proteins such as CD43, CD44, and ICAM-1/2/3 (Tsukita et al., 1994; Helander et al., 1996; Serrador et al., 1997; Yonemura et al., 1998, 1999; Shaw, 2001). These NH_2-terminal halves are also indirectly associated with membrane transporters/channels such as the Na^+/H^+ exchanger 3, CFTR (cystic fibrosis transmembrane conductance regulator), β2-adrenergic receptor, and PDGF-receptor, via a cytoplasmic phosphoprotein, EBP50/NHE-RF (Reczek et al., 1997; Yun et al., 1997; Murthy et al., 1998; Short et al., 1998; Maudsley et al., 2000; Bretscher et al., 2002). The cross-linking activity of ERM proteins between actin filaments and plasma membranes is thought to be regulated by PIP_2 in the downstream of Rho (Hirao et al., 1996; Mackay et al., 1997; Heiska et al., 1998; Matsui et al., 1999; Yonemura et al., 2002).

The suppression of ERM protein expression in lymphocytes using antisense oligonucleotides results in the complete disappearance of microvilli, suggesting that they play an essential role in cortical microvilli formation (Takeuchi et al., 1994). To examine the physiological functions of ERM proteins at the entire body level (Ingraffea et al., 2002), moesin- and radixin-deficient mice have been generated (Doi et al., 1999; Kikuchi et al., 2002). Moesin-deficient mice showed no abnormalities when examined under laboratory conditions (Doi et al., 1999). By contrast, radixin deficiency caused congenital conjugated hyperbilirubinemia with losses of multidrug resistance protein 2, a bilirubin transporter, from the bile canalicular membranes of the hepatocytes with concomitant decrease of microvilli in number as well as in length (Kikuchi et al., 2002). In wild-type mice, radixin was the dominant ERM protein in the hepatocytes, and was not substituted by either ezrin or moesin in $Rdx^{-/-}$ mice.

Taking all of the above into consideration, it would seem important that the possible involvement of ERM proteins in the formation, maintenance, and functions of stereocilia on hair cells be examined. In this work, we found that radixin was the only detectable species of ERM protein in the stereocilia of the cochlea of adult wild-type mice, whereas vestibular stereocilia appeared to contain a detectable amount of ezrin in addition to radixin. Adult $Rdx^{-/-}$ mice exhibited profound deafness, but not imbalance; consistent with this, stereocilia were significantly defective in the outer and inner hair cells of the cochlea, but not in the hair cells of the vestibule. Furthermore, we found that in the cochlea of $Rdx^{-/-}$ mice, ezrin-based stereocilia appeared to develop normally from birth to postnatal day 14 (P14), the onset of hearing, after which they progressively degenerated. Thus, the radixin knockout provides a type of mouse deafness model caused by mutation in cytoskeletal components in stereocilia, which presents with progressive degeneration of cochlear (but not vestibular) stereocilia. The present paper provides a new insight into the ERM-based molecular mechanisms for the formation and maintenance of stereocilia, and the functional specificity/redundancy among ERM proteins in situ.

Results

Radixin is specifically enriched in stereocilia in the cochlear and vestibular sensory hair cells in adult wild-type mice

As a first step to examine the possible involvement of ERM proteins in the formation/maintenance of stereocilia on hair cells, the organ of Corti and the crista ampullaris of the vestibule were isolated from adult wild-type mice aged 5 wk, and then whole-mount stained with ezrin-, radixin-, and moesin-specific mAbs (Kondo et al., 1997; Doi et al., 1999). In the organ of Corti, only radixin was concentrated both in one row of the inner hair cell stereocilia and three rows of the outer hair cell stereocilia (Fig. 1, a–c): Individual stereocilia appeared resolved both by radixin staining in immunofluorescence microscopy (Fig. 1 d) and by scanning EM (Fig. 1 e). In addition to such intense signals, diffuse weak staining for ezrin and radixin was also detected in both hair and sup-

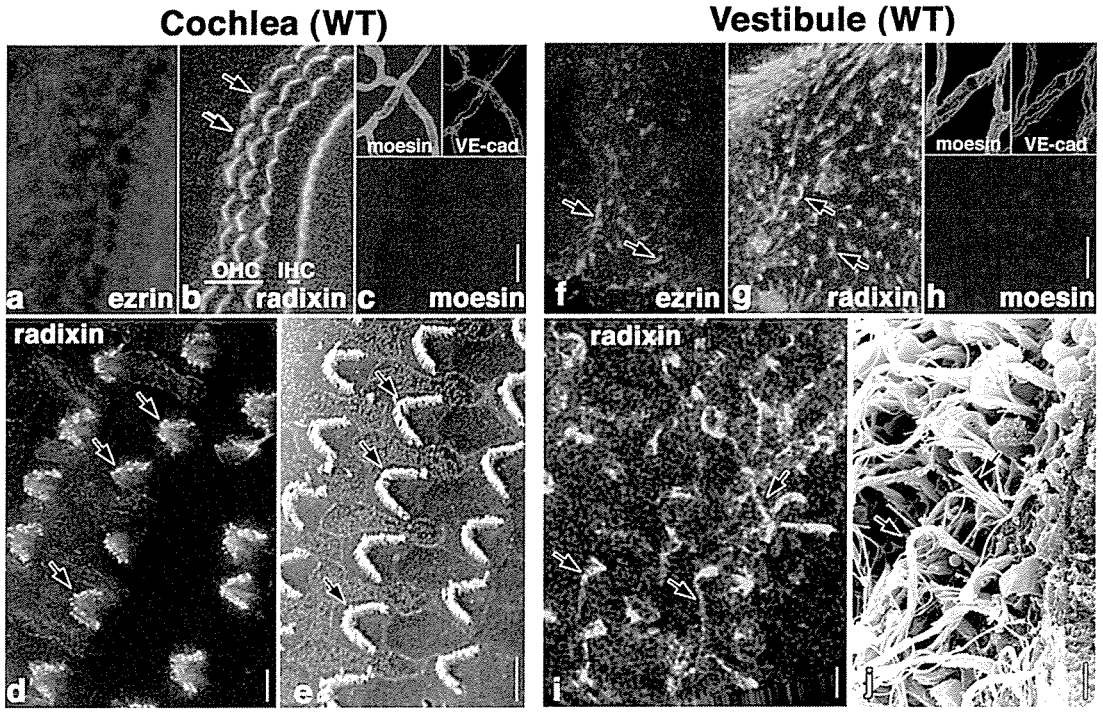

Figure 1. **ERM proteins in the cochlea and vestibule in adult wild-type mice at the age of 5 wk.** (a–c) Whole-mount immunofluorescence micrographs of the organ of Corti isolated from the cochlea with mAbs specific for ezrin, radixin, or moesin. The stereocilia of inner hair cells (IHC) and outer hair cells (OHC) are intensely stained with anti-radixin mAb (arrows). Ezrin and moesin are undetectable in the stereocilia, though moesin (moesin; green) is detected in large amounts in VE-cadherin–positive blood vessel endothelial cells (VE-cad; red) at a different focus plane (inset). Bar, 15 μm. (d and e) Comparison of the whole-mount radixin staining image with the scanning electron microscopic image of stereocilia on outer hair cells. Both radixin immunostaining (d) and scanning EM (e) reveal a highly organized array of stereocilia (arrows). Bars, 5 μm. (f–h) Whole-mount immunofluorescence micrographs of the crista ampullaris isolated from the vestibule with mAbs specific for ezrin, radixin, or moesin. Stereocilia are intensely stained with anti-radixin mAb, and weakly but reproducibly stained with anti-ezrin mAb (arrows). Moesin is detected only in the blood vessels at a different focus plane from radixin/ezrin-positive stereocilia (inset), as judged by the double-staining images for moesin (moesin; green) and VE-cadherin (VE-cad; red, inset). Bar, 15 μm. (i and j) Comparison of the whole-mount radixin staining image with the scanning electron microscopic image of stereocilia on vestibular hair cells. Radixin appears to concentrate along the entire length of long fragile stereocilia. Bars, 3 μm.

porting cells of the organ of Corti, whereas moesin was not detected in either; instead it was concentrated in the VE-cadherin–positive blood vessels (Berryman et al., 1993). In the crista ampullaris of the vestibule, radixin was concentrated in the stereocilia of the hair cells, but ezrin was also detectable in stereocilia, though faintly (Fig. 1, f–h). At higher magnification, individual long fragile vestibular stereocilia were also resolved both by radixin staining in immunofluorescence microscopy (Fig. 1 i) and by scanning EM (Fig. 1 j). Moesin was detected only in the VE-cadherin–positive blood vessels. These results indicated that radixin is the dominant ERM protein in the hair cell stereocilia of the inner ear, although the degree of contribution of ezrin appeared to be different between the cochlear and vestibular stereocilia.

Radixin deficiency causes deafness

Thus, it would be interesting to examine the physiological roles of radixin in hearing and balance in mice. First, we focused on the hearing ability of radixin-deficient ($Rdx^{-/-}$) mice. These mice showed a normal growth rate (Fig. 2 A) and were fertile, although they suffered from congenital conjugated hyperbilirubinemia (Kikuchi et al., 2002). Interestingly, when a sound stimulus was administrated in the form of a loud handclap, adult $Rdx^{-/-}$ mice (5–10-wk-old) showed no reflexive reaction, so-called Preyer's reflex, although $Rdx^{+/+}$ and $Rdx^{+/-}$ mice quickly moved their heads (Fig. 2 A). The auditory-evoked brainstem response (ABR) was then measured in two sets of heterogeneous $Rdx^{+/-}$ intercross adult littermates aged 5 and 10 wk (12 littermates in total) in response to a stimuli with a sound pressure level (SPL) of 70 decibels (dB) (20 kHz; Fig. 2 B). Of the 12 littermates, three showed no ABR; the others all showed a typical ABR waveform. Afterwards, these mice were genotyped, and these three littermates showing no ABR were all found to be $Rdx^{-/-}$ mice. This perfect correlation between the $Rdx^{-/-}$ genotype and a lack of ABR was reproducibly obtained in different series of measurements. In Fig. 2 C, the hearing thresholds of 10-wk-old mice were measured at various sound frequencies. Wild-type and $Rdx^{+/-}$ mice showed normal hearing thresholds (10–50 dB SPL), whereas $Rdx^{-/-}$ mice showed profound deafness (hearing threshold, >70–90 dB SPL).

Then, we compared light microscopic images of toluidine blue–stained sections prepared from Epon-embedded tissues of the inner ear between $Rdx^{+/+}$ and $Rdx^{-/-}$ P60 mice (Fig.

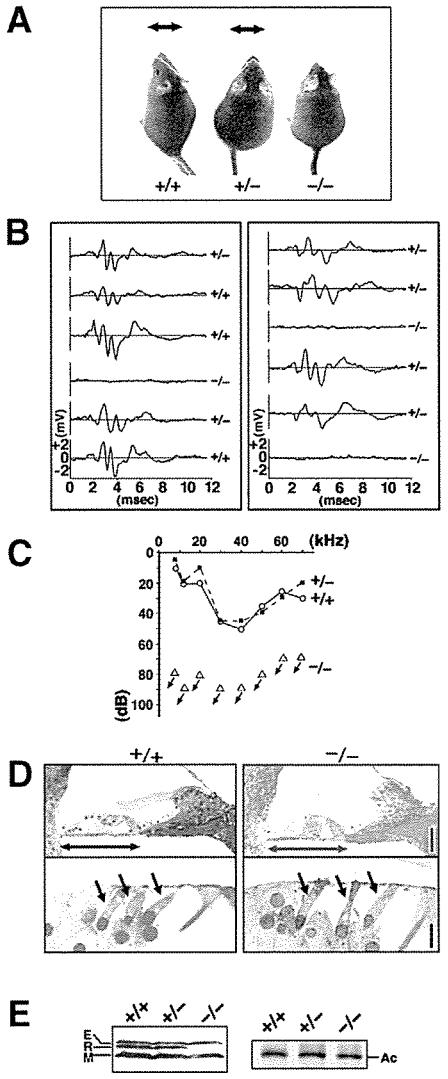

Figure 2. **Deafness of *Rdx*$^{-/-}$ mice.** (A) Loss of Preyer's reflex in *Rdx*$^{-/-}$ mice. Time-lapse photography captures Preyer's reflex in *Rdx*$^{+/+}$ and *Rdx*$^{+/-}$ mice, head movements (arrows), but not in *Rdx*$^{-/-}$ mice. Two successive frames after a loud handclap (1-s interval) were superimposed. These 10-wk-old mice show similar growth rates. (B) ABR to stimuli of 70-dB SPL (20 kHz) in two sets of *Rdx*$^{+/-}$ intercross littermates (left, 5-wk-old; right 10-wk-old). Among 12 littermates in total, three show no ABR, and were afterwards genotyped as *Rdx*$^{-/-}$ mice (blue squares). (C) Hearing thresholds of 10-wk-old *Rdx*$^{+/+}$, *Rdx*$^{+/-}$, and *Rdx*$^{-/-}$ mice at various sound frequencies. *Rdx*$^{+/+}$ and *Rdx*$^{+/-}$ mice show normal hearing thresholds (10–50 dB SPL), whereas *Rdx*$^{-/-}$ mice show profound deafness (hearing threshold, >70–90 dB SPL). (D) Toluidine blue–stained Epon semi-thin sections of the cochlea. No gross morphological difference is observed in the organ of Corti (double-headed arrows) including hair cells (single-headed arrows) between *Rdx*$^{+/+}$ and *Rdx*$^{-/-}$ mice. Bars, 50 μm (top panels); 10 μm (bottom panels). (E) Western blot analysis of isolated cochleae of the *Rdx*$^{+/+}$, *Rdx*$^{+/-}$, and *Rdx*$^{-/-}$ mice with anti-ERM pAb (TK89) that recognizes ezrin (E), radixin (R), and moesin (M) equally. In the *Rdx*$^{-/-}$ cochlea, radixin becomes undetectable without significant up-regulation of ezrin or moesin. Silver-stained bands of actin (Ac) in the same gels are present to show that an equal amount of cell lysate was applied in each lane.

2 D): No obvious gross morphological malformations were observed in *Rdx*$^{-/-}$ cochlea including hair cells, which was consistent with the scanning electron microscopic observation (see Fig. 3 A). However, as *Rdx*$^{-/-}$ mice became much older (>90 d), hair cells appeared to begin to be eliminated, leaving a fairly disorganized cell architecture of the organ of Corti (unpublished data). The expression of ERM proteins were examined in the *Rdx*$^{+/+}$, *Rdx*$^{+/-}$, and *Rdx*$^{-/-}$ cochleae isolated from P40 adult littermates by Western blotting with anti-ERM pAb (Fig. 2 E). Ezrin, radixin, and moesin were detected in both *Rdx*$^{+/+}$ and *Rdx*$^{+/-}$ cochleae, but *Rdx*$^{-/-}$ cochlea lacked radixin expression specifically and showed no significant up-regulation of ezrin or moesin.

Radixin deficiency causes progressive degeneration of stereocilia of cochlear hair cells after the onset of hearing

The question then naturally arose as to what is the consequence of radixin deficiency in the cochlear stereocilia in *Rdx*$^{-/-}$ mice. Isolated cochleae of P40 *Rdx*$^{+/+}$ and *Rdx*$^{-/-}$ littermates were examined by scanning EM (Fig. 3 A, a–f). When removing the lateral wall and tectorial membrane of the cochlea in P40 *Rdx*$^{-/-}$ mice to expose the organ of Corti, the cellular arrangement of the outer and inner hair cells as well as the supporting cells appeared normal, but very interestingly, the stereocilia in both outer and inner hair cells were significantly defective compared with those in *Rdx*$^{+/+}$ organ of Corti. Instead of being regularly arranged in a "W" shape, stereocilia of the outer hair cells of *Rdx*$^{-/-}$ mice were deformed to 1–3 residual knoblike protrusions on the apical surfaces (Fig. 3 A, d). Inner hair cells had several shorter fused protrusions instead of stereocilia (Fig. 3 A, f). When the organ of Corti isolated from these *Rdx*$^{-/-}$ cochleae was whole-mount stained with ezrin-, radixin-, and moesin-specific mAbs, ezrin, radixin, or moesin was not detected in the residual structures of outer and inner stereocilia, i.e., knoblike protrusions and shorter fused protrusions, respectively (Fig. 3 A, g–j). Diffuse ezrin staining in the organ of Corti and intense moesin staining in blood vessels did not appear to be affected. Considering that stereocilia play a central role in transducing acoustic stimuli into electrical signals in the cochlea, it is likely that these defects in cochlear stereocilia are responsible for the hearing impairments observed in adult *Rdx*$^{-/-}$ mice.

Cochlear hair cells of mice were reported to continue to develop after birth, and to become functionally mature at the onset of hearing around the age of 14 d (Lim and Anniko, 1985; Erven et al., 2002; Zuo, 2002). Therefore, we next attempted to distinguish whether in *Rdx*$^{-/-}$ mice cochlear stereocilia are defective in their development or degenerate after they have developed normally. As previously reported (Lim and Anniko, 1985; Zuo, 2002), in the cochleae of wild-type P1 mice, scanning EM showed that both the inner and outer hair cells already bore well-developed stereocilia in a characteristic arrangement (Fig. 3 B, a, c, and e). The central tubulin-based kinocilium of the W-shaped array of stereocilia on inner hair cells were especially prominent at this early stage. In addition to stereocilia, at this stage hair cells as well as supporting cells were covered with a large

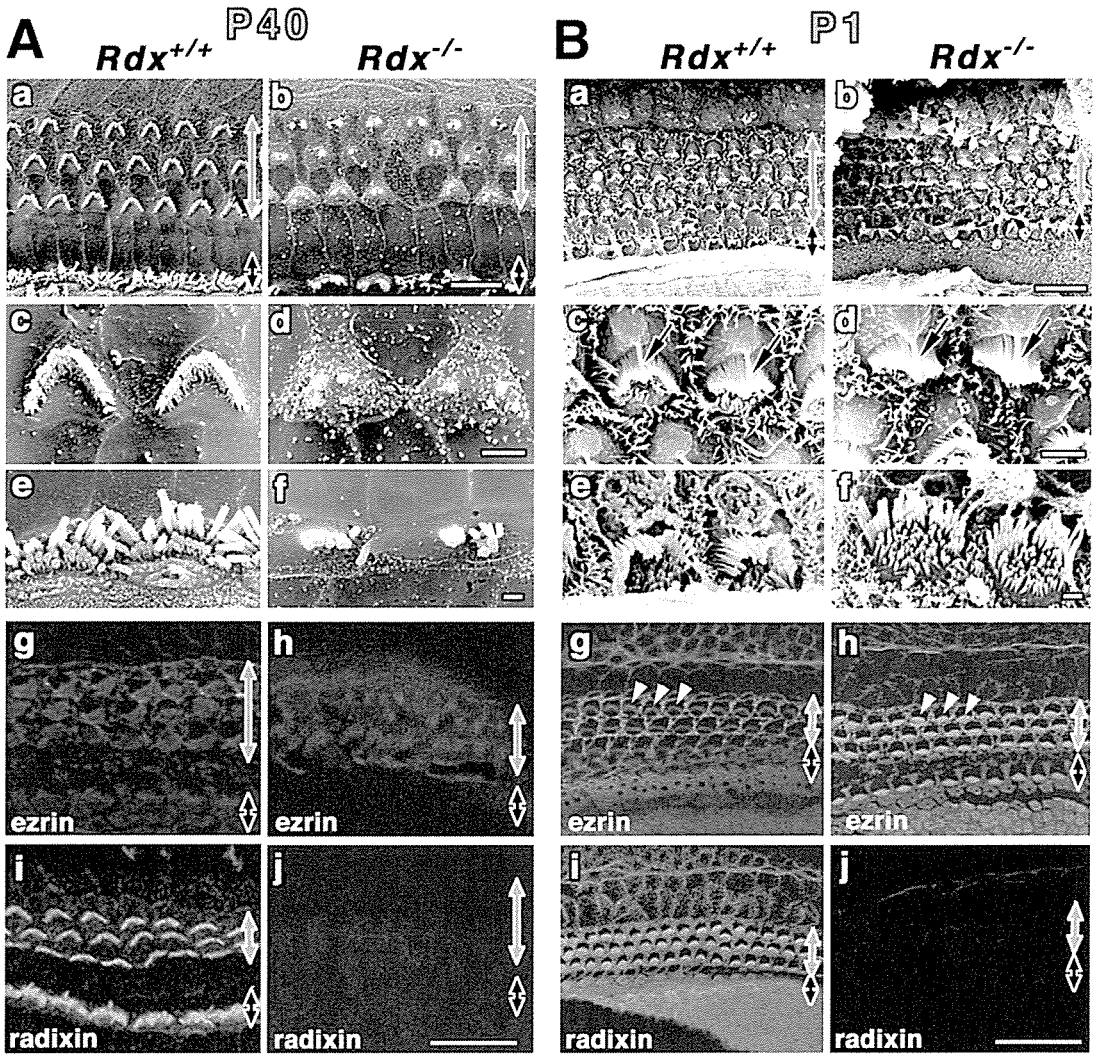

Figure 3. **Stereocilia on $Rdx^{+/+}$ and $Rdx^{-/-}$ cochlear hair cells of adult and newborn mice.** (A) Scanning electron micrographs (a–f) and whole-mount immunofluorescence micrographs for radixin and ezrin (g–j) of the $Rdx^{+/+}$ and $Rdx^{-/-}$ organ of Corti at 40 d of age (P40). The levels of outer hair cells (blue arrows) and inner hair cells (black arrows) are shown. At low magnification in the scanning electron micrograph of the $Rdx^{+/+}$ organ of Corti (a), the luminal surface is characterized by three rows of outer hair cells (blue arrow) and one row of inner hair cells (black arrow). Outer hair cells bear stereocilia arranged regularly in the form of a letter W (c), and inner hair cells have more disorganized arrays of stereocilia (e). In the $Rdx^{-/-}$ organ of Corti (b), no significant abnormalities are detected in the cellular arrangements on the luminal surface, but the morphology of the stereocilia on both the outer (blue arrow) and inner (black arrow) hair cells is severely affected. In $Rdx^{-/-}$ outer hair cells, instead of regularly arranged stereocilia, 1–3 residual knoblike protrusions are observed on their apical surface (d). $Rdx^{-/-}$ inner hair cells bear several shorter fused irregularly shaped protrusions instead of long stereocilia (f). By immunostaining, in the $Rdx^{-/-}$ organ of Corti (h and j), no staining for radixin is detected without any increase in the staining intensities for ezrin. Bars, 10 μm (a and b); 2 μm (c and d); 1 μm (e and f); 20 μm (g–j). (B) Scanning electron micrographs (a–f) and whole-mount immunofluorescence micrographs for radixin and ezrin (g–j) of the $Rdx^{+/+}$ and $Rdx^{-/-}$ organ of Corti at 1 d of age (P1). Scanning electron microscopic images of the cochlea of P1 $Rdx^{-/-}$ mice (b, d, and f) are indistinguishable from those in the $Rdx^{+/+}$ mice (a, c, and e). In addition to stereocilia arrays carrying central tubulin-based kinocilium (arrows in c and d), hair cells as well as supporting cells are covered with large numbers of short conventional microvilli that have mostly disappeared in adult mice. Whole-mount immunostaining reveals that in the P1 $Rdx^{+/+}$ organ of Corti, radixin is highly enriched in stereocilia of inner and outer hair cells as well as the apical surface of hair and supporting cells (i), but in contrast to adult mice ezrin is also detected in stereocilia, weakly but clearly (g, arrowheads). In the $Rdx^{-/-}$ organ of Corti, instead of radixin, ezrin is highly concentrated at stereocilia on both inner and outer hair cells (h, arrowheads). Bars, 10 μm (a and b); 2 μm (c and d); 1 μm (e and f); 20 μm (g–j).

number of short conventional microvilli that disappeared in adult mice (Fig. 3 A). To our surprise, the scanning electron microscopic images of the cochlea of P1 $Rdx^{-/-}$ mice were indistinguishable from those in the $Rdx^{+/+}$ mice (Fig. 3 B, b, d, and f). The question is how stereocilia were developed normally in the absence of radixin in P1 $Rdx^{-/-}$ mice. Whole-mount immunostaining was then performed (Fig. 3 B, g–j). In P1 $Rdx^{+/+}$ mice, radixin was highly enriched in stereocilia of inner and outer hair cells, but in contrast to adult mice, ezrin was also detected in stereocilia, weakly but clearly (Fig. 3 B, g and i). Furthermore, the P1 $Rdx^{+/+}$ cochlea was characterized by punctate radixin and ezrin signals

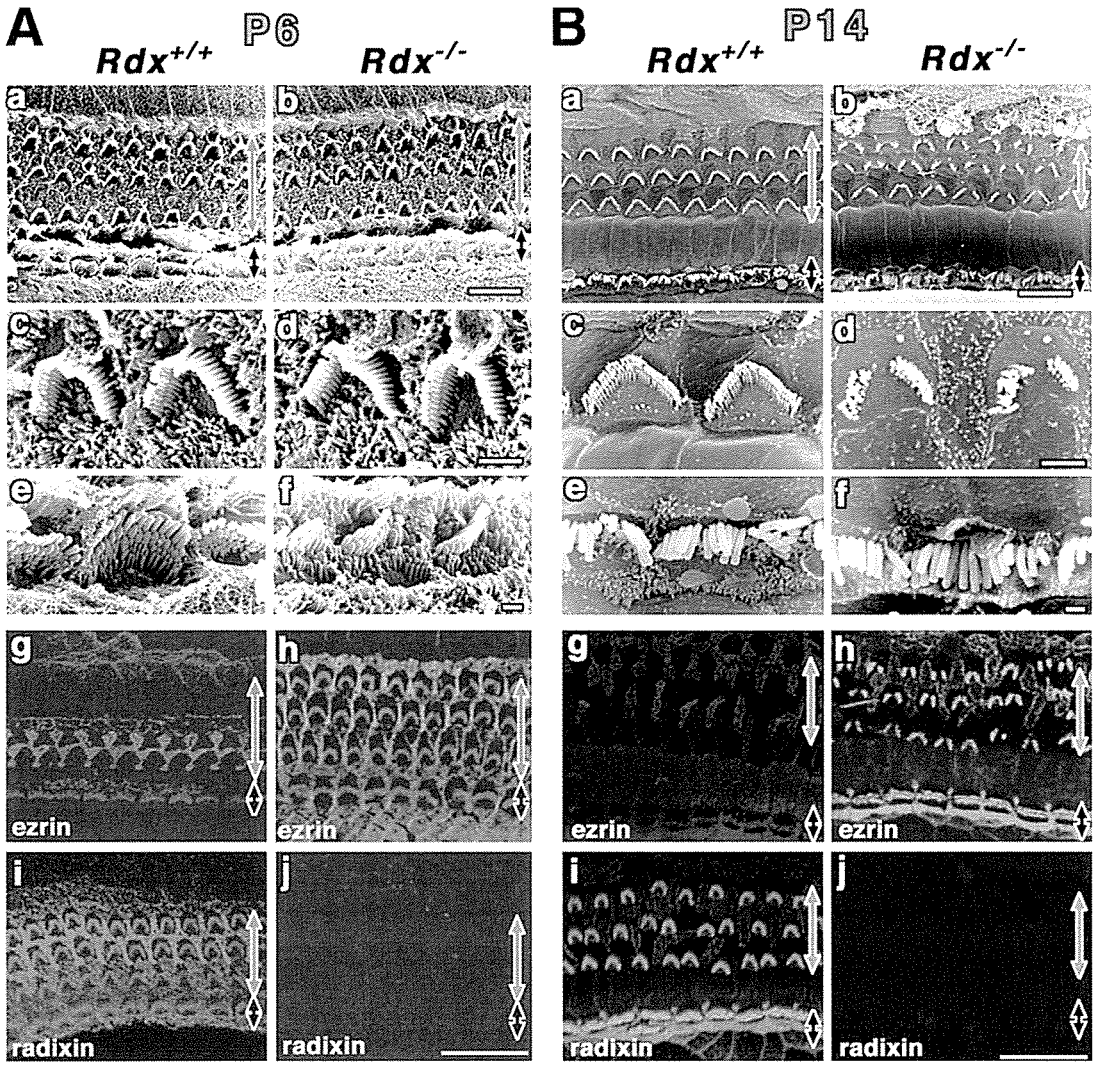

Figure 4. **Postnatal degeneration of stereocilia on *Rdx*$^{-/-}$ cochlear hair cells.** (A) Scanning electron micrographs (a–f) and whole-mount immunofluorescence micrographs for radixin and ezrin (g–j) of the organ of Corti isolated from *Rdx*$^{+/+}$ and *Rdx*$^{-/-}$ mice at 6 d of age (P6). The levels of outer hair cells (blue arrows) and inner hair cells (black arrows) are shown. Scanning EM does not detect any significant differences between *Rdx*$^{+/+}$ (a, c, and e) and *Rdx*$^{-/-}$ cochlea (b, d, and f). In contrast to P1 *Rdx*$^{+/+}$ cochlea, in P6 *Rdx*$^{+/+}$ cochlea, whole-mount immunostaining detects a weak signal of ezrin at radixin-enriched stereocilia on inner hair cells (black arrow), and a trace of ezrin in outer hair cells (blue arrow) (g and i). In *Rdx*$^{-/-}$ cochlea (h and j), ezrin is still highly concentrated at stereocilia on both inner hair cells (black arrow) and outer hair cells (blue arrow). Bars, 10 μm (a and b); 2 μm (c and d); 1 μm (e and f); 20 μm (g–j). (B) Scanning electron micrographs (a–f) and whole-mount immunofluorescence micrographs for radixin and ezrin (g–j) of the organ of Corti isolated from *Rdx*$^{+/+}$ and *Rdx*$^{-/-}$ mice at 14 d of age (P14). Scanning EM detects the initial sign for the degeneration of stereocilia on outer hair cells (blue arrow) (a–d). The central part of the W-shaped row of stereocilia is lost, leaving discontinuous and disorganized arrays of stereocilia in *Rdx*$^{-/-}$ cochlea. At this stage, no significant defects can be observed in stereocilia on the inner hair cells (black arrow) (b and f). In P14 *Rdx*$^{+/+}$ cochlea, ezrin is only weakly detected at radixin-enriched stereocilia on inner hair cells (black arrow), and is not detected in outer hair cells (blue arrow) (g and i). In *Rdx*$^{-/-}$ cochlea, ezrin was still concentrated in the degenerating stereocilia in large amounts in outer and inner hair cells (h). Bars, 10 μm (a and b); 2 μm (c and d); 1 μm (e and f); 20 μm (g–j).

on the apical surface of hair cells and supporting cells, which may correspond to numerous conventional microvilli. Of course, in the organ of Corti in P1 *Rdx*$^{-/-}$ littermates, radixin was undetectable (Fig. 3 B, j), but instead of radixin, ezrin was markedly increased in stereocilia of both inner and outer hair cells as well as in conventional microvilli on hair and supporting cells (Fig. 3 B, h). Therefore, ezrin appeared to compensate for radixin deficiency in the development of hair cell stereocilia, at least up to 1 d after birth. Subsequently, these ezrin-based stereocilia degenerated postnatally.

We then pursued the possible postnatal degeneration process of stereocilia in *Rdx*$^{-/-}$ mice (Fig. 4). At P6, scanning EM did not detect any significant differences between *Rdx*$^{+/+}$ and *Rdx*$^{-/-}$ cochlea, indicating that there was still no sign for stereocilia degeneration (Fig. 4 A, a–f). However, in *Rdx*$^{+/+}$ cochlea, ezrin became weaker during P1 to P14, almost undetectable from stereocilia at ~P14, and radixin was

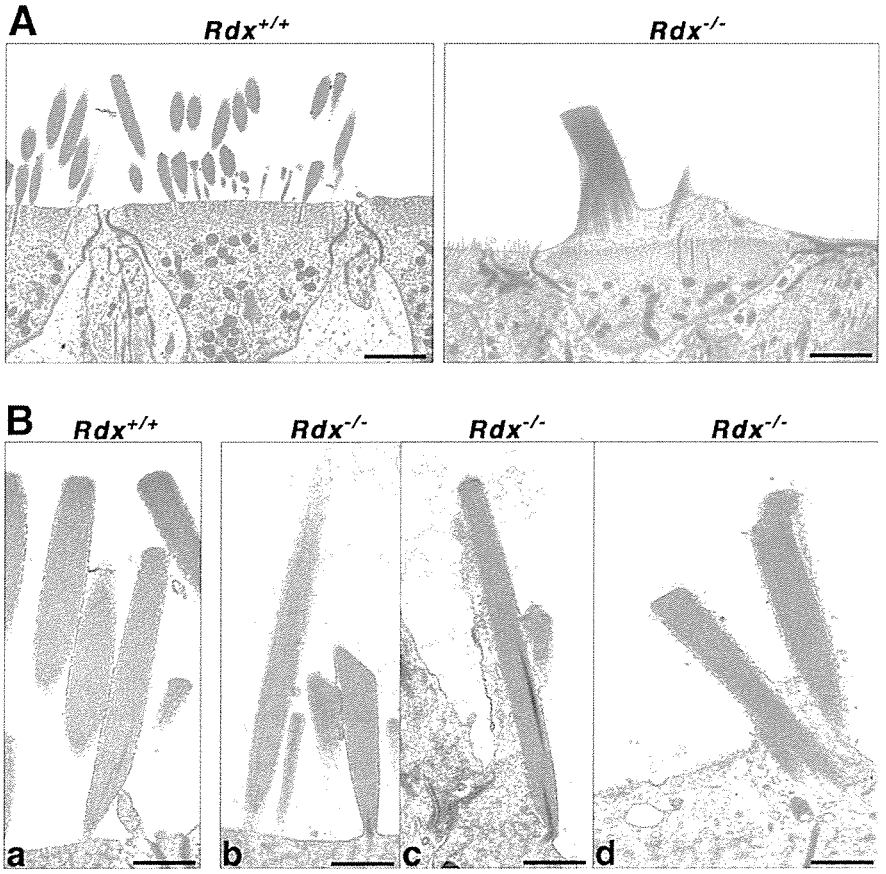

Figure 5. **Ultrathin-section electron micrographs of stereocilia of cochlear outer hair cells of *Rdx*$^{+/+}$ and *Rdx*$^{-/-}$ mice aged 3 wk.** (A) Low power electron micrographs. All of the *Rdx*$^{+/+}$ hair cells bear numerous stereocilia with normal appearance, whereas *Rdx*$^{-/-}$ hair cells were frequently characterized by abnormal 1–3 residual knoblike cellular protrusions on their apical surfaces. These images may correspond to the scanning electron micrographs of Fig. 3 A, c and d, respectively. Bars, 2 μm. (B) *Rdx*$^{+/+}$ radixin-based stereocilia (a) and *Rdx*$^{-/-}$ ezrin-based stereocilia at various degeneration stages (b–d). *Rdx*$^{-/-}$ ezrin-based stereocilia contained highly-organized bundles of actin filaments as cores (b) that were indistinguishable in appearance from those in *Rdx*$^{+/+}$ radixin-based stereocilia (a), and during the process of degeneration, these stereocilia as well as core bundles appeared to be fused to form abnormal thick and short protrusions (c and d). Bars, 0.5 μm.

dominantly detected among ERM proteins in stereocilia (Fig. 4 A, g and i). Supporting cells were intensely stained for ezrin and radixin. In P6 *Rdx*$^{-/-}$ cochlea, ezrin was highly concentrated in stereocilia on both inner and outer hair cells (Fig. 4 A, h) with no radixin staining (Fig. 4 A, j). Around age P14 (onset of hearing in mice), in *Rdx*$^{-/-}$ cochlea, the sign for stereocilia degeneration began to be detected on outer hair cells by scanning EM (Fig. 4 B, a–f): The central part of the W-shaped row of stereocilia was lost, leaving discontinuous and disorganized arrays of stereocilia. Ezrin was still concentrated in these degenerating stereocilia in large amounts, though in *Rdx*$^{+/+}$ hair cells, radixin, but not ezrin, was enriched at stereocilia (Fig. 4 B, g–j). We concluded that in *Rdx*$^{-/-}$ cochleae, ezrin can counterbalance radixin deficiency to normally develop stereocilia up to the onset of hearing, but not to maintain these once-developed stereocilia to transmit acoustic stimuli into electrical signals.

To clarify the interior structure of ezrin-based stereocilia in *Rdx*$^{-/-}$ cochleae, the cochleae of *Rdx*$^{-/-}$ mice aged 3 wk were examined by ultrathin-section EM (Fig. 5). In these mice, stereocilia at various stages of degeneration were observed. Ezrin-based stereocilia contained highly organized bundles of actin filaments as cores that were indistinguishable in appearance from those in wild-type radixin-based stereocilia, and during the process of degeneration these stereocilia as well as core bundles appeared to be fused to form abnormal thick and short protrusions.

Finally, a natural question is what are the membrane-binding partners for radixin/ezrin in cochlear stereocilia. To elucidate an answer, we first performed immunoprecipitation experiments with anti-radixin or anti-ezrin mAb using isolated *Rdx*$^{+/+}$ or *Rdx*$^{-/-}$ cochlea; however, the results were inconclusive, probably due to the limitation of the material and the low insolubility of radixin and ezrin. We also performed a gel overlay blot with labeled radixin/ezrin, but again failed to detect any bands specifically associated with radixin/ezrin.

Ezrin compensates radixin deficiency in the development/maintenance of stereocilia in the vestibular hair cells

As shown in Fig. 1, in the vestibule of wild-type mice aged 5–10 wk, radixin was predominantly concentrated in stereocilia among ERM proteins, but distinct from cochlear stereocilia, these stereocilia contained detectable amounts of ezrin. The question then arose as to the structure and function of vestibular stereocilia in adult *Rdx*$^{-/-}$ mice. Structurally, scanning EM identified no abnormality in the number/density and morphology of stereocilia at the crista ampullaris of the vestibule of adult *Rdx*$^{-/-}$ mice (Fig. 6 A). Also, scanning EM identified no abnormality in the otolith organs (the utricle and saccule) of adult *Rdx*$^{-/-}$ mice (unpublished data). Functionally, *Rdx*$^{-/-}$ vestibular stereocilia appeared to be normal because adult *Rdx*$^{-/-}$ mice showed no signs of imbalance in their behavior as far as we examined up to 100 d after birth. Then, their vestibulo-ocular reflex (VOR) was measured, in which the function of horizontal semicircular canals, but not otolith organs (the utricle and saccule), can be evaluated. Heads of *Rdx*$^{+/+}$, *Rdx*$^{+/-}$, or *Rdx*$^{-/-}$ mice aged

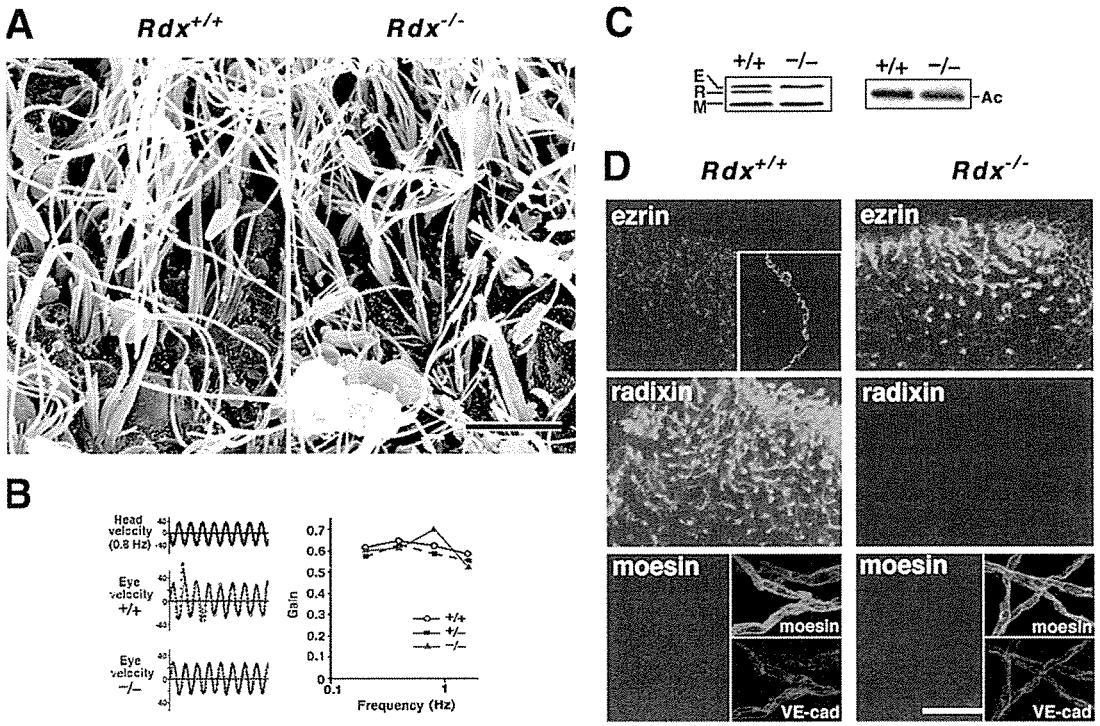

Figure 6. **The vestibule and the balance function of 5-wk-old *Rdx*$^{-/-}$ mice.** (A) Scanning EM of the *Rdx*$^{+/+}$ and *Rdx*$^{-/-}$ crista ampullaris of the vestibule. The appearance of stereocilia (arrows) was indistinguishable between *Rdx*$^{+/+}$ and *Rdx*$^{-/-}$ mice. Bar, 5 μm. (B) VOR. A mouse head was rotated sinusoidally and the eye position recorded by a CCD camera (left). The eye velocity was calculated from the change of eye position, and was fitted with sinusoidal curves (red lines). The gain was obtained by dividing the peak eye velocity by the peak head velocity. No difference is detected in the VOR between *Rdx*$^{+/+}$ and *Rdx*$^{-/-}$ mice. The VOR gains of *Rdx*$^{-/-}$ mice are also normal at any frequency of the head rotation stimulus in *Rdx*$^{+/+}$ and *Rdx*$^{-/-}$ mice (right). (C) Western blot analysis of isolated *Rdx*$^{+/+}$ and *Rdx*$^{-/-}$ vestibule (mainly crista ampullaris) with anti-ERM pAb (TK89) that recognizes ezrin, radixin, and moesin with almost the same affinity. In *Rdx*$^{-/-}$ vestibule, radixin (R) became undetectable without significant up-regulation of ezrin (E) or moesin (M). Silver-stained bands of actin (Ac) are presented on the right to show that equal amounts of cell lysate were applied in each lane. (D) Whole-mount immunostaining of the crista ampullaris isolated from the *Rdx*$^{+/+}$ and *Rdx*$^{-/-}$ vestibules with ezrin-, radixin- and moesin-specific antibodies. In the *Rdx*$^{+/+}$ crista ampullaris, radixin is highly concentrated in the stereocilia where ezrin is detected weakly but reproducibly (inset, a frozen section stained with anti-ezrin antibody). Moesin is detected only in the blood vessels at a different focus plane from stereocilia (inset), as judged by the double staining images for moesin (moesin; green) and VE-cadherin (VE-cad; red) (inset). By contrast, in the *Rdx*$^{-/-}$ crista ampullaris, the concentration of ezrin in the stereocilia is significantly increased. All samples were treated under completely identical conditions, paying special attention to ensure that the signals were not saturated. Bar, 40 μm.

~5–10 wk were rotated sinusoidally and eye positions were recorded using a CCD camera at various head rotation frequencies. As shown in Fig. 6 B, the VOR gains of *Rdx*$^{-/-}$ mice were normal at all head rotation frequencies.

Western blotting of the isolated vestibule with anti-ERM pAb revealed no significant up-regulation of ezrin or moesin in adult *Rdx*$^{-/-}$ mice (Fig. 6 C). We then whole-mount stained the crista ampullaris isolated from adult *Rdx*$^{+/+}$ and *Rdx*$^{-/-}$ vestibule with ezrin-, radixin-, and moesin-specific mAbs (Fig. 6 D). In the vestibule of *Rdx*$^{+/+}$ mice, radixin was specifically and highly enriched in the stereocilia of the crista ampullaris with a small amount of ezrin, whereas in the *Rdx*$^{-/-}$ crista ampullaris, instead of radixin, ezrin was highly concentrated in stereocilia, although this up-regulation of ezrin in stereocilia could not be detected by immunoblotting of the whole vestibule (Fig. 6 C). Therefore, in the vestibule, ezrin appears to be able to compensate radixin deficiency not only in developing stereocilia, but also in maintaining them to transmit acceleration stimuli into electrical signals.

Discussion

The physiological functions of ERM proteins, ezrin, radixin, and moesin, have attracted increasing interest, but the relevance of the existence of these three closely related proteins in mammalian cells remains elusive (Berryman et al., 1993; Takeuchi et al., 1994; Doi et al., 1999; Tsukita and Yonemura, 1999; Ingraffea et al., 2002; Kikuchi et al., 2002). In most cultured mammalian cells, all ERM proteins are coexpressed and codistributed (Sato et al., 1992; Berryman et al., 1993). Using antisense oligonucleotides, ERM proteins were shown to be functionally redundant, without a quantitatively compensatory increase in their expression levels, in cell–cell/cell–substrate adhesion and the formation of microvilli in cultured cells (Takeuchi et al., 1994). At the whole-body level, the expression levels and combinations of ERM proteins varied significantly depending on cell type (Sato et al., 1992; Berryman et al., 1993; Franck et al., 1993; Doi et al., 1999; Ingraffea et al., 2002), and to date no clear example has been found to indicate the functional

redundancy among ERM proteins. Radixin deficiency causes hyperbilirubinemia due to the loss of multidrug resistance protein 2 from the bile canalicular membranes, where microvilli were decreased in number as well as in length (Kikuchi et al., 2002). Radixin was the dominant ERM protein in the liver of wild-type mice, but no compensatory up-regulation of expression level of ezrin or moesin was detected in the $Rdx^{-/-}$ liver.

To discuss the functions of ERM proteins and their possible redundancy in situ, the inner ear provides an advantageous system, as in it there are two distinct types of stereocilia, cochlear and vestibular stereocilia, which play central roles in transmitting acoustic and acceleration stimuli, respectively, into electrical signals. (Roberts et al., 1988; Hudspeth, 1989; Pickles and Corey, 1992; Eatock et al., 1998; Corey, 2003). In wild-type cochlea, before ~P14, ezrin was detectable in addition to large amounts of radixin in stereocilia, and then progressively disappeared, leaving purely radixin-based stereocilia. In the $Rdx^{-/-}$ cochlea, ezrin was significantly up-regulated, and purely ezrin-based stereocilia developed normally up to ~P14 and then progressively degenerated. By contrast, in the $Rdx^{+/+}$ vestibule, stereocilia contained a small amount of ezrin in addition to large amounts of radixin throughout life, whereas in the $Rdx^{-/-}$ vestibule, stereocilia containing up-regulated ezrin developed and was maintained normally throughout the life. These findings would provide the first clear example that these members of the ERM family, ezrin and radixin, function redundantly in situ at the whole-body level: ezrin compensates for radixin deficiency functionally in stereocilia. In $Rdx^{+/+}$ mice, the cochlear hair cells up to ~P14 and the vestibular hair cells throughout the life expressed both radixin and ezrin in large and small amounts, respectively, and probably due to the difference in their expression levels or affinity to plasma membranes, radixin was the main contributor to the formation of stereocilia. In these hair cells, in the absence of radixin ($Rdx^{-/-}$ mice), a larger amount of ezrin was recruited, which appeared to compensate for radixin deficiency in the formation of stereocilia.

The molecular mechanism behind the progressive degeneration of the cochlear stereocilia after the onset of hearing (~P14) remained elusive. At present, two explanations appear possible. First, if the expression of ezrin is genetically programmed to be suppressed in cochlear hair cells after the onset of hearing in the wild-type mice, and if this program is not changed by radixin deficiency, in $Rdx^{-/-}$ mice, cochlear hair cells lack both ezrin and radixin after the onset of hearing, resulting in progressive degeneration of stereocilia. As the total lack of ERM proteins was reported to cause cell death (Kondo et al., 1997), this mechanism can explain why cochlear hair cells were eliminated in older $Rdx^{-/-}$ mice. The second possibility is that sound stimulation induces the progressive degeneration of ezrin-based stereocilia in the $Rdx^{-/-}$ cochlea. It would be possible that these ezrin-based stereocilia are more labile against the noise stimulation (i.e., frequent deflection) than the wild-type radixin-based stereocilia due to the qualitative or quantitative difference between radixin in wild-type stereocilia and ezrin in $Rdx^{-/-}$ stereocilia. Consistently, the noise-induced loss of stereocilia was reported in the wild-type mice as well as humans (Ou et al., 2000). As deflection frequency for vestibular stereocilia is expected to be much lower than for cochlear stereocilia, $Rdx^{-/-}$ vestibule ezrin-based stereocilia could be maintained without degeneration. According to Western blotting of the whole cochlea and vestibule, there were no signs for up-regulation of the expression of ezrin (or moesin), but as it was technically difficult to examine the expression of ERM proteins in individual sensory hair cells, the two above explanations cannot be further evaluated for now. Furthermore, to understand the molecular mechanism behind the progressive degeneration of the cochlear stereocilia, identification of the specific molecular partners of radixin and ezrin, including integral membrane proteins, within stereocilia would be important, although it is again technically difficult due to the small number of stereocilia in the cochlea. Indeed, as described in the results, we performed immunoprecipitation and gel overlay experiments, but were unable to identify the radixin- or ezrin-binding partners in stereocilia. To be successful, any future work will need to overcome several technical difficulties.

Mutations in the actin-bundling protein espin have been reported in *jerker* mice and DFNB36, a form of nonsyndromic deafness in humans (Grüneberg et al., 1941; Zheng et al., 2000; Belyantseva et al., 2003). Adult *jerker* mice exhibit impaired hearing and balance dysfunctions, as well as short cochlear and vestibular stereocilia. Analyses of various aged *jerker* mice revealed apparently normal cochlear stereocilia development until the onset of hearing, after which the stereocilia progressively degenerate (Sjöström and Anniko, 1992). This aspect of *jerker* mice is very similar to $Rdx^{-/-}$ mice, but *jerker* mice are completely different from $Rdx^{-/-}$ mice in terms of the balance dysfunction. Because espin is likely to play a role in bundling actin filaments in stereocilia (Loomis et al., 2003), it was suggested that the organization of core actin filaments is critical for the maintenance of stereocilia after the onset of hearing. Furthermore, genetic studies of deafness in mice and humans have identified several genes for other cytoskeleton-related proteins, harmonin, myosin VI/VIIa, whirlin, and SANS, and for cadherin-related proteins, cadherin 23 and protocadherin 15, as causal genes (Avraham et al., 1995; Gibson et al., 1995; Probst et al., 1998; Self et al., 1998; Littlewood Evans and Müller, 2000; Zheng et al., 2000; Alagramam et al., 2001; Di Palma et al., 2001: Petit et al., 2001; Boeda et al., 2002; Mustapha et al., 2002; Karolyi et al., 2003; Kikkawa et al., 2003; Mburu et al., 2003; Weil et al., 2003). In these mice, the formation of not only cochlear, but also vestibular stereocilia was affected, resulting in the deafness associated with imbalance. All these cytoskeleton-related proteins, including ERM proteins and epsin, may act in cooperative ways to form and maintain dynamic stereocilia in cochlear and vestibular sensory hair cells.

To date, three mouse models in which there is profound hearing loss and no vestibular dysfunction have been reported: the deafness (dn) gene mutant mice (Bock and Steel, 1983), Beethoven mice (Vreugde et al., 2002), and the claudin 14-knockout mice (Ben-Yosef et al., 2003). $Rdx^{-/-}$ mice can now be added as a new member of this list. $Rdx^{-/-}$ mice should provide a valuable resource for further analysis of the functional redundancy of ERM proteins at the whole-body level, and of the molecular mechanisms behind the formation and maintenance of highly specialized microvilli, stereocilia;

the elucidation of which will shed light on the pathogenesis of human deafness and imbalance.

Materials and methods

Antibodies

Rabbit anti-ERM pAb, TK89, recognized COOH-terminal domains of all ERM proteins almost equally (Kondo et al., 1997; Doi et al., 1999). We previously raised and characterized rat anti-ezrin (M11), anti-radixin (R21), and anti-moesin mAb (M22) (Kondo et al., 1997; Doi et al., 1999). Goat anti-VE-cadherin (C-19) was obtained from Santa Cruz Biotechnology, Inc.

Generation of $Rdx^{-/-}$ mice

Rdx$^{-/-}$ mice were generated as previously reported (Kikuchi et al., 2002). Two independent mouse J1 ES clones (129/Sv) in which the radixin gene was correctly disrupted were injected into C57BL/6 blastocysts, and the resulting chimeras were mated with C57BL/6 mice (Doi et al., 1999).

ABR measurements

ABR measurements were performed in a soundproof room (Zheng et al., 1999). In general, the ABR waveforms were recorded for 12.8 ms at a sampling rate of 40,000 Hz using 50–5,000-Hz filter settings; waveforms recorded from 1,024 stimuli at a frequency of 9 Hz were averaged. ABR waveforms were recorded in decreasing 5-dB SPL intervals from a maximum amplitude until no waveforms could be visualized.

VOR measurements

VOR was measured as described by Iwashita et al. (2001). Head movements were transduced to DC signals using a small angular velocity sensor (Gyrostar; Murata Corporation) that was fixed on the turntable. Eye movements were detected by LED and a CCD camera (C53500; Tokyo Electronic Industry), and eye velocities were calculated online by downloading them onto a computer through a video capture board. Both the head and eye velocity curves were fitted with sinusoidal curves using the least squares criterion, and the gain of eye velocity relative to the head velocity was obtained.

Immunofluorescence microscopy

Temporal bones were removed from 1-, 6-, 14-, or 40-d-old mice, and together with the small holes in the cochlear apical turn and superior semicircular canal, the round and oval windows were opened. The lymphatic space was gently perfused with 10% TCA through a round window (Hayashi et al., 1999; Kitajiri et al., 2004). Samples were then immersed in 10% TCA for 1 h at 4°C, washed three times with PBS, and decalcified with 5% EDTA in PBS for 3 d at 4°C. The cochlea and vestibule were then carefully microdissected, treated with 0.2% Triton X-100 in PBS for 15 min, and soaked in 1% BSA in PBS at RT. They were then incubated with rat anti-ezrin (M11), anti-radixin (R11), or anti-moesin (M22) mAb for 30 min at RT. Samples were washed three times with PBS, followed by a 30-min incubation with Cy3- (Jackson ImmunoResearch Laboratories, Inc.) or Alexa Fluor® 488–conjugated secondary antibody (Molecular Probes, Inc.). After a wash with PBS, they were embedded in 95% glycerol-PBS containing 0.1% paraphenylendiamine and 1% *n*-propylgalate. Fluorescence images were obtained with a confocal microscope (model LSM 510 META; Carl Zeiss MicroImaging, Inc.) or with a DeltaVision optical sectioning microscope (version 2.10; Applied Precision, Inc.), equipped with an Axioplan2 (Plan Apochromat 63×/1.40 NA oil immersion objective; Carl Zeiss MicroImaging, Inc.) or IX70 (PlanApo 60×/1.40 NA oil immersion objective; Olympus) microscope, respectively.

Immunoblotting

The membranous labyrinths of 5-wk-old mice were dissected under a microscope. Whole organ of Corti and vestibules isolated from each mouse were sonicated in 100 μl SDS sample buffer (50 mM Tris-HCl, pH 6.8, 2% SDS, 20% glycerol, 2% 2-mercaptoethanol, and 0.01% bromophenol blue), applied to SDS-PAGE, and immunoblotted by a blotting detection kit with biotinylated Ig and streptavidin-conjugated alkaline phosphatase (Amersham Biosciences).

Scanning EM

Temporal bones obtained from 1-, 6-, 14-, or 40-d-old mice were fixed using perilymphatic perfusion as described above with 1% glutaraldehyde in 0.1 M phosphate buffer (pH 7.2). They were then washed with phosphate buffer and post-fixed in 1% OsO_4 for 2 h, after which they were once again treated with perilymphatic perfusion. The organ of Corti or crista ampullaris was microdissected, dehydrated, critical-point dried, sputter coated, and observed by scanning EM (model S-800 microscope; Hitachi Co.).

Ultrathin-section EM

Samples were processed as previously described, using 2% formaldehyde, 2.5% glutaraldehyde, and 0.1 M sodium cacodylate buffer (pH 7.4) as a fixative (Yonemura et al., 2002).

We would like to thank Drs. E. Kikuchi, T.S. Kim, H. Saito, and N. Yamamoto (Kyoto University) for technical help and advice.

This work was supported in part by a Grant-in-Aid for Cancer Research and a Grant-in-Aid for Scientific Research (A) from the Ministry of Education, Science and Culture, Japan to Shoichiro Tsukita, and in part by a Grant-in-Aid for Scientific Research (B) from the Ministry of Education, Science and Culture, Japan, to Sachiko Tsukita.

Submitted: 2 February 2004
Accepted: 14 June 2004

Note added in proof. While this paper was being reviewed, Pataky et al. presented evidence that radixin is a constituent of stereocilia in hair cells (Pataky, F., R. Pironkova, and A.J. Hudspeth. 2004. *Proc. Natl. Acad. Sci. USA.* 101:2601–2606).

References

Alagramam, K.N., C.L. Murcia, H.Y. Kwon, K.S. Pawlowski, C.G. Wright, and R.P. Woychik. 2001. The mouse Ames waltzer hearing-loss mutant is caused by mutation of *Pcdh15*, a novel protocadherin gene. *Nat. Genet.* 27: 99–102.

Algrain, M., O. Turunen, A. Vaheri, D. Louvard, and M. Arpin. 1993. Ezrin contains cytoskeleton and membrane binding domains accounting for its proposed role as a membrane-cytoskeletal linker. *J. Cell Biol.* 120:129–140.

Avraham, K.B., T. Hasson, K.P. Steel, D.M. Kingsley, L.B. Russell, M.S. Mooseker, N.G. Copeland, and N.A. Jenkins. 1995. The mouse Snell's waltzer deafness gene encodes an unconventional myosin required for structural integrity of inner ear hair cells. *Nat. Genet.* 11:369–375.

Bartles, J.R. 2000. Parallel actin bundles and their multiple actin-bundling proteins. *Curr. Opin. Cell Biol.* 12:72–78.

Belyantseva, I.A., V. Labay, E.T. Boger, A.J. Griffith, and T.B. Friedman. 2003. Stereocilia: the long and the short of it. *Trends Mol. Med.* 9:458–461.

Ben-Yosef, T., I.A. Belyantseva, T.L. Saunders, E.D. Hughes, K. Kawamoto, C.M. Van Itallie, L.A. Beyer, K. Halsey, D.J. Gardner, E.R. Wilcox, et al. 2003. Claudin 14 knockout mice, a model for autosomal recessive deafness DFNB29, are deaf due to cochlear hair cell degeneration. *Hum. Mol. Genet.* 12:2049–2061.

Berryman, M., Z. Franck, and A. Bretscher. 1993. Ezrin is concentrated in the apical microvilli of a wide variety of epithelial cells whereas moesin is found primarily in endothelial cells. *J. Cell Sci.* 105:1025–1043.

Bock, G.R., and K.P. Steel. 1983. Inner ear pathology in the *deafness* mutant mouse. *Acta Otolaryngol.* 96:39–47.

Boeda, B., A. El-Amraoui, A. Bahloul, R. Goodyear, L. Daviet, S. Blanchard, I. Perfettini, K.R. Fath, S. Shorte, J. Reiners, et al. 2002. Myosin VIIa, harmonin and cadherin 23, three Usher I gene products that cooperate to shape the sensory hair cell bundle. *EMBO J.* 21:6689–6699.

Bretscher, A., K. Edwards, and R.G. Fehon. 2002. ERM proteins and merlin: integrators at the cell cortex. *Nat. Rev. Mol. Cell Biol.* 3:586–599.

Call, L.M., and C.C. Morton. 2002. Continuing to break the sound barrier: genes in hearing. *Curr. Opin. Genet. Dev.* 12:343–348.

Corey, D. 2003. Sensory transduction in the ear. *J. Cell Sci.* 116:1–3.

Denman-Johnson, K., and A. Forge. 1999. Establishment of hair bundle polarity and orientation in the developing vestibular system of the mouse. *J. Neurocytol.* 28:821–835.

DeRosier, D.J., and L.G. Tilney. 2000. F-actin bundles are derivatives of microvilli: What does this tell us about how bundles might form? *J. Cell Biol.* 148:1–6.

DeRosier, D.J., L.G. Tilney, and E. Egelman. 1980. Actin in the inner ear: the remarkable structure of the stereocilium. *Nature.* 287:291–296.

Di Palma, F., R.H. Holme, E.C. Bryda, I.A. Belyantseva, R. Pellegrino, B. Kachar, K.P. Steel, and K. Noben-Trauth. 2001. Mutations in Cdh23, encod-

ing a new type of cadherin, cause stereocilia disorganization in waltzer, the mouse model for Usher syndrome type 1D. *Nat. Genet.* 27:103–107.

Doi, Y., M. Itoh, S. Yonemura, S. Ishihara, H. Takano, T. Noda, Sh. Tsukita, and Sa. Tsukita. 1999. Normal development of mice and unimpaired cell adhesion/cell motility/actin-based cytoskeleton without compensatory up-regulation of ezrin or radixin in moesin gene knockout. *J. Biol. Chem.* 274: 2315–2321.

Drenckhahn, D., K. Engel, D. Höfer, C. Merte, L. Tilney, and M. Tilney. 1991. Three different actin filament assemblies occur in every hair cell: each contains a specific actin crosslinking protein. *J. Cell Biol.* 112:641–651.

Dumont, R.A., Y.D. Zhao, J.R. Holt, M. Bahler, and P.G. Gillespie. 2002. Myosin-I isozymes in neonatal rodent auditory and vestibular epithelia. *J. Assoc. Res. Otolaryngol.* 3:375–389.

Eatock, R.A., A. Rusch, A. Lysakowski, and M. Saeki. 1998. Hair cells in mammalian utricles. *Otolaryngol. Head Neck Surg.* 119:172–181.

Erven, A., M.J. Skynner, K. Okumura, S. Takebayashi, S.D.M. Brown, K.P. Steel, and N.D. Allen. 2002. A novel stereocilia defect in sensory hair cells of the deaf mouse mutant Tasmanian devil. *Eur. J. Neurosci.* 16:1433–1441.

Fortnum, H., and A. Davis. 1997. Epidemiology of permanent childhood hearing impairment in Trent Region, 1985–1993. *Br. J. Audiol.* 31:409–446.

Franck, Z., R. Gary, and A. Bretscher. 1993. Moesin, like ezrin, colocalizes with actin in the cortical cytoskeleton in cultured cells, but its expression is more variable. *J. Cell Sci.* 105:219–231.

Furukawa, R., and M. Fechheimer. 1997. The structure, function, and assembly of actin filament bundles. *Int. Rev. Cytol.* 175:29–90.

Gibson, F., J. Walsh, P. Mburu, A. Varela, K.A. Brown, M. Antonio, K.W. Beisel, K.P. Steel, and S.D. Brown. 1995. A type VII myosin encoded by the mouse deafness gene shaker-1. *Nature.* 374:62–64.

Gillespie, P.G., and R.G. Walker. 2001. Molecular basis of mechanosensory transduction. *Nature.* 413:194–202.

Grüneberg, H., J.B. Burnett, and G.D. Snell. 1941. The origin of jerker, a new gene mutation of the house mouse, and linkage studies made with it. *Proc. Natl. Acad. Sci. USA.* 27:562–565.

Hayashi, K., S. Yonemura, T. Matsui, Sa. Tsukita, and Sh. Tsukita. 1999. Immunofluorescence detection of ezrin/radixin/moesin (ERM) proteins with their carboxyl-terminal threonine phosphorylated in cultured cells and tissues. *J. Cell Sci.* 112:1149–1158.

Heiska, L., K. Alfthan, M. Gröholm, P. Vilja, A. Vaheri, and O. Carpén. 1998. Association of ezrin with intercellular adhesion molecule-1 and -2 (ICAM-1 and ICAM-2). Regulation by phosphatidylinositol 4,5-bisphosphate. *J. Biol. Chem.* 273:21893–21900.

Helander, T.S., O. Carpén, O. Turunen, P.E. Kovanen, A. Vaheri, and T. Timonen. 1996. ICAM-2 redistributed by ezrin as a target for killer cells. *Nature.* 382:265–268.

Henry, M.D., C. Gonzalez Agosti, and F. Solomon. 1995. Molecular dissection of radixin: distinct and interdependent functions of the amino- and carboxy-terminal domains. *J. Cell Biol.* 129:1007–1022.

Hirao, M., N. Sato, T. Kondo, S. Yonemura, M. Monden, T. Sasaki, Y. Takai, Sh. Tsukita, and Sa. Tsukita. 1996. Regulation mechanism of ERM (ezrin/radixin/moesin) protein/plasma membrane association: possible involvement of phosphatidylinositol turnover and Rho-dependent signaling pathway. *J. Cell Biol.* 135:37–51.

Holme, R.H., and K.P. Steel. 1999. Genes involved in deafness. *Curr. Opin. Genet. Dev.* 9:309–314.

Hudspeth, A.J. 1989. How the ear's works work. *Nature.* 341:397–404.

Ingraffea, J., D. Reczek, and A. Bretscher. 2002. Distinct cell type-specific expression of scaffolding proteins EBP50 and E3KARP: EBP50 is generally expressed with ezrin in specific epithelia, whereas E3KARP is not. *Eur. J. Cell Biol.* 81:61–68.

Iwashita, M., R. Kanai, K. Funabiki, K. Matsuda, and T. Hirano. 2001. Dynamic properties, interactions and adaptive modifications of vestibulo-ocular reflex and optokinetic response in mice. *Neurosci. Res.* 39:299–311.

Karolyi, I.J., F.J. Probst, L. Beyer, H. Odeh, G. Dootz, K.B. Cha, D.M. Martin, K.B. Avraham, D. Kohrman, D.F. Dolan, et al. 2003. Myo15 function is distinct from Myo6, Myo7a and pirouette genes in development of cochlear stereocilia. *Hum. Mol. Genet.* 12:2797–2805.

Kikkawa, Y., H. Shitara, S. Wakana, Y. Kohara, T. Takada, M. Okamoto, C. Taya, K. Kamiya, Y. Yoshikawa, H. Tokano, et al. 2003. Mutations in a new scaffold protein *Sans* cause deafness in Jackson shaker mice. *Hum. Mol. Genet.* 12:453–461.

Kikuchi, S., M. Hata, K. Fukumoto, Y. Yamane, T. Matsui, A. Tamura, S. Yonemura, H. Yamagishi, D. Keppler, Sh. Tsukita, and Sa. Tsukita. 2002. Radixin deficiency causes conjugated hyperbilirubinemia with loss of Mrp2 from bile canalicular membranes. *Nat. Genet.* 31:320–325.

Kitajiri, S., M. Furuse, K. Morita, Y. Saishin-Kiuchi, H. Kido, J. Ito, and Sh. Tsukita. 2004. Expression patterns of claudins, tight junction adhesion molecules, in the inner ear. *Hear. Res.* 187:25–34.

Kondo, T., K. Takeuchi, Y. Doi, S. Yonemura, S. Nagata, Sh. Tsukita, and Sa. Tsukita. 1997. ERM (ezrin/radixin/moesin)-based molecular mechanism of microvillar breakdown at an early stage of apoptosis. *J. Cell Biol.* 139:749–758.

Liang, Y., A. Wang, I.A. Belyantseva, D.W. Anderson, F.J. Probst, T.D. Barber, W. Miller, J.W. Touchman, L. Jin, S.L. Sullivan, et al. 1999. Characterization of the human and mouse unconventional myosin XV genes responsible for hereditary deafness. *Genomics.* 61:243–258.

Lim, D.J., and M. Anniko. 1985. Developmental morphology of the mouse inner ear. A scanning electron microscopic observation. *Acta Otolaryngol. Suppl.* 422:1–69.

Littlewood Evans, A., and U. Müller. 2000. Stereocilia defects in the sensory hair cells of the inner ear in mice deficient in integrin $\alpha 8\beta 1$. *Nat. Genet.* 24:424–428.

Loomis, P.A., L. Zheng, G. Sekerkova, B. Changyaleket, E. Mugnaini, and J.R. Bartles. 2003. Espin cross-links cause the elongation of microvillus-type parallel actin bundles in vivo. *J. Cell Biol.* 163:1045–1055.

Mackay, D.J.G., F. Esch, H. Furthmayr, and A. Hall. 1997. Rho- and rac-dependent assembly of focal adhesion complexes and actin filaments in permeabilized fibroblasts: an essential role for ezrin/radixin/moesin proteins. *J. Cell Biol.* 138:927–938.

Mangeat, P., C. Roy, and M. Martin. 1999. ERM proteins in cell adhesion and membrane dynamics. *Trends Cell Biol.* 9:187–192.

Martin, M., C. Andréoli, A. Sahuquet, P. Montcourrier, M. Algrain, and P. Mangeat. 1995. Ezrin NH_2-terminal domain inhibits the cell extension activity of the COOH-terminal domain. *J. Cell Biol.* 128:1081–1093.

Matsui, T., S. Yonemura, Sh. Tsukita, and Sa. Tsukita. 1999. Activation of ERM proteins in vivo by Rho involves phosphatidyl-inositol 4-phosphate 5-kinase and not ROCK kinases. *Curr. Biol.* 9:1259–1262.

Maudsley, S., A.M. Zamah, N. Rahman, J.T. Blitzer, L.M. Luttrell, R.J. Lefkowitz, and R.A. Hall. 2000. Platelet-derived growth factor receptor association with Na^+/H^+ exchanger regulatory factor potentiates receptor activity. *Mol. Cell. Biol.* 20:8352–8363.

Mburu, P., M. Mustapha, A. Varela, D. Weil, A. El-Amraoui, R.H. Holme, A. Rump, R.E. Hardisty, S. Blanchard, R.S. Coimbra, et al. 2003. Defects in whirlin, a PDZ domain molecule involved in stereocilia elongation, cause deafness in the whirler mouse and families with DFNB31. *Nat. Genet.* 34: 421–428.

Morton, N.E. 1991. Genetic epidemiology of hearing impairment. *Ann. NY Acad. Sci.* 630:16–31.

Murthy, A., C. Gonzalez-Agosti, E. Cordero, D. Pinney, C. Candia, F. Solomon, J. Gusella, and V. Ramesh. 1998. NHE-RF, a regulatory cofactor for Na^+-H^+ exchange, is a common interactor for merlin and ERM (MERM) proteins. *J. Biol. Chem.* 273:1273–1276.

Mustapha, M., E. Chouery, D. Torchard-Pagnez, S. Nouaille, A. Khrais, F.N. Sayegh, A. Megarbane, J. Loiselet, M. Lathrop, C. Petit, and D. Weil. 2002. A novel locus for Usher syndrome type I, USH1G, maps to chromosome 17q24-25. *Hum. Genet.* 110:348–350.

Ou, H.C., B.A. Bohne, and G.W. Harding. 2000. Noise damage in the C57BL/CBA mouse cochlea. *Hear. Res.* 145:111–122.

Petit, C., J. Levilliers, and J.P. Hardelin. 2001. Molecular genetics of hearing loss. *Annu. Rev. Genet.* 35:589–646.

Pickles, J.O., and D.P. Corey. 1992. Mechanoelectrical transduction by hair cells. *Trends Neurosci.* 15:254–259.

Probst, F.J., and S.A. Camper. 1999. The role of mouse mutants in the identification of human hereditary hearing loss genes. *Hear. Res.* 130:1–6.

Probst, F.J., R.A. Fridell, Y. Raphael, T.L. Saunders, A. Wang, Y. Liang, R.J. Morell, J.W. Touchman, R.H. Lyons, K. Noben-Trauth, et al. 1998. Correction of deafness in *shaker-2* mice by an unconventional myosin in a BAC transgene. *Science.* 280:1444–1447.

Reczek, D., M. Berryman, and A. Bretscher. 1997. Identification of EBP50: A PDZ-containing phosphoprotein that associates with members of the ezrin-radixin-moesin family. *J. Cell Biol.* 139:169–179.

Roberts, W.M., J. Howard, and A.J. Hudspeth. 1988. Hair cells: transduction, tuning, and transmission in the inner ear. *Annu. Rev. Cell Biol.* 4:63–92.

Sato, N., N. Funayama, A. Nagafuchi, S. Yonemura, Sa. Tsukita, and Sh. Tsukita. 1992. A gene family consisting of ezrin, radixin and moesin. Its specific localization at actin filament/plasma membrane association sites. *J. Cell Sci.*

103:131–143.

Self, T., M. Mahony, J. Fleming, J. Walsh, S.D. Brown, and K.P. Steel. 1998. Shaker-1 mutations reveal roles for myosin VIIA in both development and function of cochlear hair cells. *Development.* 125:557–566.

Serrador, J. M., J.L. Alonso-Lebrero, M.A. del Pozo, H. Furthmayr, R. Schwartz-Albiez, R.J. Calvo, F. Lozano, and F. Sánchez-Madrid. 1997. Moesin interacts with the cytoplasmic region of intercellular adhesion molecule-3 and is redistributed to the uropod of T lymphocytes during cell polarization. *J. Cell Biol.* 138:1409–1423.

Shaw, A.S. 2001. FERMing up the synapse. *Immunity.* 15:683–686.

Short, D.B., K.W. Trotter, D. Reczek, S.M. Kreda, A. Bretscher, R.C. Boucher, M.J. Stutts, and S.L. Milgram. 1998. An apical PDZ protein anchors the cystic fibrosis transmembrane conductance regulator to the cytoskeleton. *J. Biol. Chem.* 273:19797–19801.

Sjöström, B., and M. Anniko. 1992. Genetically induced inner ear degeneration. A structural and functional study. *Acta Otolaryngol. Suppl.* 493:141–146.

Skowron, J.F., W.M. Bement, and M.S. Mooseker. 1998. Human brush border myosin-I and myosin-Ic expression in human intestine and Caco-2_{BBe} cells. *Cell Motil. Cytoskeleton.* 41:308–324.

Sobin, A., and A. Flock. 1983. Immunohistochemical identification and localization of actin and fimbrin in vestibular hair cells in the normal guinea pig and in a strain of the waltzing guinea pig. *Acta Otolaryngol.* 96:407–412.

Steel, K.P., and C.J. Kros. 2001. A genetic approach to understanding auditory function. *Nat. Genet.* 27:143–149.

Takeuchi, K., N. Sato, H. Kasahara, N. Funayama, A. Nagafuchi, S. Yonemura, Sa. Tsukita, and Sh. Tsukita. 1994. Perturbation of cell adhesion and microvilli formation by antisense oligonucleotides to ERM family members. *J. Cell Biol.* 125:1371–1384.

Tekin, M., K.S. Arnos, and A. Pandya. 2001. Advances in hereditary deafness. *Lancet.* 358:1082–1090.

Tilney, M.S., L.G. Tilney, R.E. Stephens, C. Merte, D. Drenckhahn, D.A. Cotanche, and A. Bretscher. 1989. Preliminary biochemical characterization of the stereocilia and cuticular plate of hair cells of the chick cochlea. *J. Cell Biol.* 109:1711–1723.

Tsukita, Sa., and S. Yonemura. 1999. Cortical actin organization: lessons from ERM (ezrin/radixin/moesin) proteins. *J. Biol. Chem.* 274:34507–34510.

Tsukita, Sa., K. Oishi, N. Sato, J. Sagara, A. Kawai, and Sh. Tsukita. 1994. ERM family members as molecular linkers between the cell surface glycoprotein CD44 and actin-based cytoskeletons. *J. Cell Biol.* 126:391–401.

Turunen, O., T. Wahlström, and A. Vaheri. 1994. Ezrin has a COOH-terminal actin-binding site that is conserved in the ezrin protein family. *J. Cell Biol.* 126:1445–1453.

Vreugde, S., A. Erven, C.J. Kros, W. Marcotti, H. Fuchs, K. Kurima, E.R. Wilcox, T.B. Friedman, A.J. Griffith, R. Balling, et al. 2002. Beethoven, a mouse model for dominant, progressive hearing loss DFNA36. *Nat. Genet.* 30:257–258.

Wada, T., Y. Wakabayashi, S. Takahashi, T. Ushiki, Y. Kikkawa, H. Yonekawa, and R. Kominami. 2001. A point mutation in a cadherin gene, *Cdh23*, causes deafness in a novel mutant, *Waltzer mouse niigata. Biochem. Biophys. Res. Commun.* 283:113–117.

Weil, D., A. El-Amraoui, S. Masmoudi, M. Mustapha, Y. Kikkawa, S. Laine, S. Delmaghani, A. Adato, S. Nadifi, Z.B. Zina, et al. 2003. Usher syndrome type I G (USH1G) is caused by mutations in the gene encoding SANS, a protein that associates with the USH1C protein, harmonin. *Hum. Mol. Genet.* 12:463–471.

Yonemura, S., M. Hirao, Y. Doi, N. Takahashi, T. Kondo, Sa. Tsukita, and Sh. Tsukita. 1998. Ezrin/radixin/moesin (ERM) proteins bind to a positively charged amino acid cluster in the juxta-membrane cytoplasmic domain of CD44, CD43, and ICAM-2. *J. Cell Biol.* 140:885–895.

Yonemura, S., Sa. Tsukita, and Sh. Tsukita. 1999. Direct involvement of ezrin/radixin/moesin (ERM)-binding membrane proteins in the organization of microvilli in collaboration with activated ERM proteins. *J. Cell Biol.* 145: 1497–1509.

Yonemura, S., T. Matsui, Sh. Tsukita, and Sa. Tsukita. 2002. Rho-dependent and -independent activation mechanisms of ezrin/radixin/moesin proteins: an essential role for polyphosphoinositides in vivo. *J. Cell Sci.* 115:2569–2580.

Yun, C.H.C., S. Oh, M. Zizak, D. Steplock, S. Tsao, C.-M. Tse, E.J. Weinman, and M. Donowitz. 1997. cAMP-mediated inhibition of the epithelial brush border Na^+/H^+ exchanger, NHE3, requires an associated regulatory protein. *Proc. Natl. Acad. Sci. USA.* 94:3010–3015.

Zheng, L., G. Sekerkova, K. Vranich, L.G. Tilney, E. Mugnaini, and J.R. Bartles. 2000. The deaf jerker mouse has a mutation in the gene encoding the espin actin-bundling proteins of hair cell stereocilia and lacks espins. *Cell.* 102: 377–385.

Zheng, Q.Y., K.R. Johnson, and L.C. Erway. 1999. Assessment of hearing in 80 inbred strains of mice by ABR threshold analyses. *Hear. Res.* 130:94–107.

Zuo, J. 2002. Transgenic and gene targeting studies of hair cell function in mouse inner ear. *J. Neurobiol.* 53:286–305.

Mini Review

内耳への神経幹細胞移植

中川隆之，井口福一郎，伊藤壽一
京都大学大学院医学研究科耳鼻咽喉科・頭頸部外科

Transplantation of neural stem cells into the inner ear
Hearing and balance disorders are included in most common disabilities, and the majority is incurable because of the low capability for regeneration of the inner ear. New therapeutic approaches including cell transplantation are therefore subjected to overcome degenerative diseases of inner ears. Firstly, transplantation of neural stem cells (NSCs) into inner ears has been attempted as well as the retina. Grafted NSCs can survive and migrate into inner ear tissues including sensory epithelia after transplantation into inner ears of newborn rats. Histological analysis following transplantation of NSCs into injured, matured inner ears of mice demonstrates the potential of NSCs for replacement of inner ear hair cells or primary neurons. *In vitro* analysis also support the hypothesis that NSCs can differentiate into inner ear hair cells. In addition, NSC-derived cells have the potential for producing several neurotrophins in the inner ear, suggesting the potential of NSC transplantation for protection of inner ear tissues from degeneration.

Rec.3/29/2004, Acc.5/12/2004, pp562-566
Takayuki Nakagawa, Fukuichiro Iguchi, Juichi Ito
Department of Otolaryngology, Head and Neck Surgery,
Kyoto University Graduate School of Medicine

Key words transplantation, inner ear, neural stem cell, regeneration, protection

はじめに

内耳は聴覚および平衡覚の末梢受容器であり，内耳障害は感音難聴，めまいの主な原因の一つとされている．高度の内耳障害は聾や高度の平衡障害を来し，日常生活を著しく障害する．これら内耳障害の頻度は決して低いものではなく，例えば感音難聴は60歳以上の人口の約60%に存在し，身体障害者に該当する高度内耳障害者は，本邦で40万人以上存在する．このように多くの高度内耳障害者が存在する要因として，内耳の脆弱性があげられる．哺乳類の内耳は，一旦傷害されると機能的に再生することは，極めて困難とされている．このような背景から，現在内耳障害に対する有効な治療法はほとんどなく，ごく限られた場合にのみ機能回復が期待できる．人工内耳は，蝸牛に電極を挿入し，ラセン神経節を有毛細胞にかわり，刺激することにより聴覚を再獲得させる医療機器として広く用いられている．しかし，適応は高度感音難聴者に限定され，また得られる聴力も自然な聴力とは異なる．

内耳における聴覚や平衡覚の受容には有毛細胞が不可欠である．有毛細胞は，音響や振動といった物理的な信号を電気信号に変換する役割を果たしている．また，有毛細胞が受容した信号を脳に伝える一次ニューロンも内耳に存在し，内耳感覚受容に不可欠な細胞である．しかし，有毛細胞とこれと連なる一次ニューロンは，哺乳類での再生は極めて困難であり，ごく限られた再生能力が前庭感覚上皮に存在することが報告されているのみである[1]．しかしながら，近年の分子生物学および幹細胞医学の発展とその内耳への応用により，哺乳類内耳再生が不可能なものでなくなりつつある．このような新しい研究の流れの一つとして，内耳への遺伝子導入がある．有毛細胞の分化運命決定機構に関係する遺伝子を感覚上皮の支持細胞に導入することにより，有毛細胞が再生することが報告されている[2,3]．しかし，機能的再生を証明する報告はなされていない．一方，内耳で再生能力が低い要因として，再生細胞の元となる幹細胞や前駆細胞といえる細胞が内

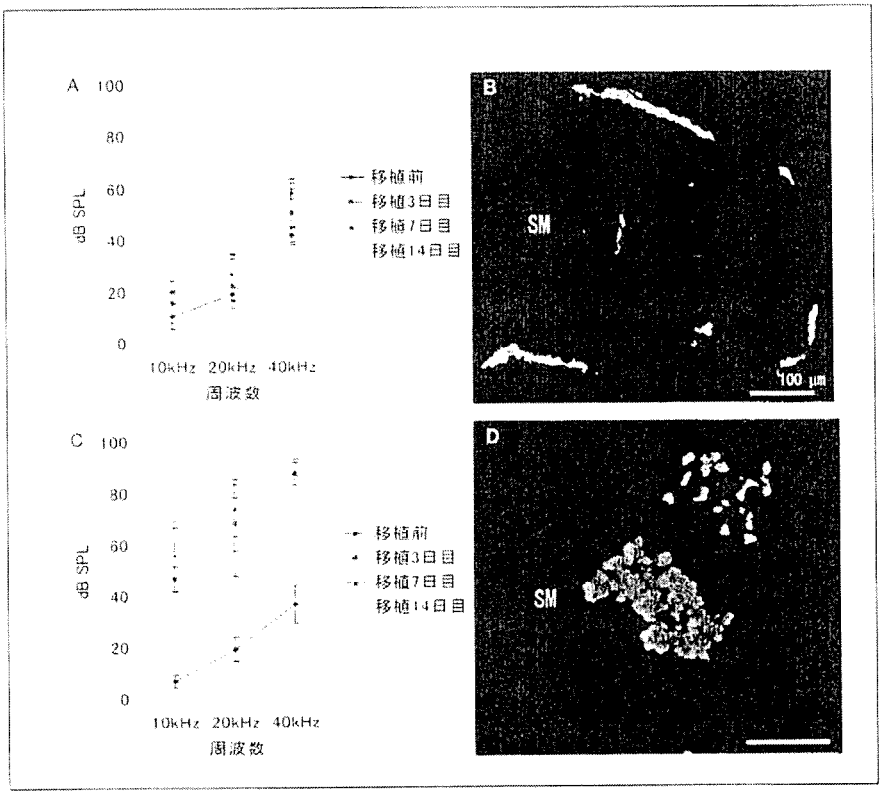

図1 マウス内耳への神経幹細胞移植後の聴力変化と蝸牛内神経幹細胞の局在

A：半規管から細胞移植後の聴覚閾値（中央値±標準偏差）の変化．閾値上昇は約10dBにとどまる．B：蝸牛第2回転での移植細胞（緑色蛍光）の局在．蝸牛内に移植細胞を認めるが，中央階（SM）には認められない．C：蝸牛から直接細胞を移植した後の聴覚閾値の変化．移植直後より約50dBの閾値上昇を認め，回復傾向を認めない．D：蝸牛から直接移植した場合，移植細胞（緑色蛍光）は中央階（SM）にも認められる．（文献11）より一部改変）

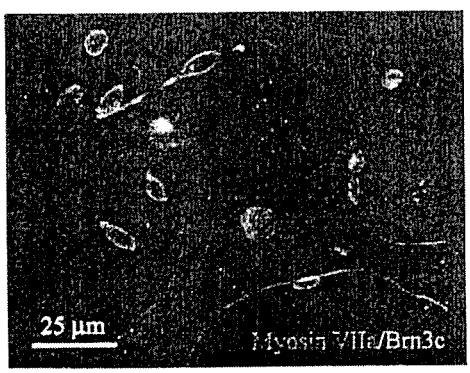

図2 神経幹細胞から誘導された有毛細胞phenotype

myosin VIIa（赤色蛍光）の発現を細胞質，Brn3c（緑色蛍光）発現を核に認める細胞を認める．（文献12)より一部改変）

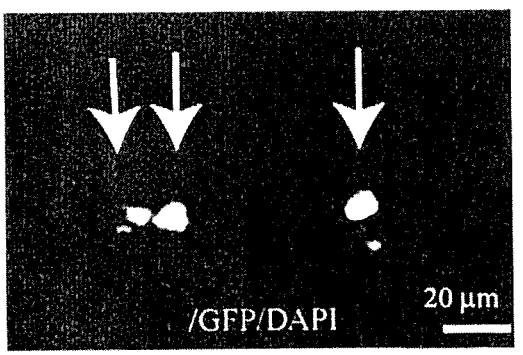

図3 前庭感覚上皮内に生着した神経幹細胞由来細胞

前庭感覚上皮内にmyosin VIIa（赤色蛍光）陽性，GFP（緑色蛍光）陽性の細胞を認める（矢印）．青色蛍光はDAPIによる核染色を示す．（文献13)より一部改変）

細胞の移行を期待する観点から，蝸牛側壁から直接細胞を注入する方法を用いた．結果，移植細胞の生着が蝸牛，前庭感覚上皮内およびラセン神経節に認められた[11]．この結果を無処置の内耳に移植した場合と比較すると，内耳組織内への神経幹細胞の移行が良好であり，内耳においても，組織傷害が移植細胞の生着に影響を及ぼすことが推察された．有毛細胞のマーカーであるmyosin VIIa陽性細胞は，前庭感覚上皮に生着した細胞にのみ認められた（図3）．したがって，内耳に移植された神経幹細胞は，内耳感覚上皮内に生着し，有毛細胞の特徴を有する細胞に分化しうることが明らかとなった．この結果は，神経幹細胞移植が内耳有毛細胞再生に応用できる可能性を示す